

Increased Functionality of Optical Fibers for Life-Science Applications

Aziza Sudirman



KTH Engineering Sciences

Doctoral Thesis
Department of Applied Physics
KTH – Royal Institute of Technology
Stockholm, Sweden 2014

*Mårten Stjernström,
my mentor, colleague and dear friend.
You left us so suddenly.
We miss you.*

Increased Functionality of Optical Fibers for Life-Science Applications

© Aziza Sudirman 2014

Quantum Electronics and Quantum Optics
Department of Applied Physics
KTH – Royal Institute of Technology
106 91 Stockholm

ISBN 978-91-7595-122-5

TRITA-FYS 2014:15

ISSN 0280-316X

ISRN KTH/FYS/--14:15—SE

Akademisk avhandling som med tillstånd av Kungliga Tekniska Högskolan framlägges till offentlig granskning för avläggande av teknologie doktorsexamen onsdagen den 21 maj, 2014, kl 10.00 i sal FD5, Albanova, Roslagstullsbacken 21, KTH, Stockholm. Avhandlingen kommer att försvaras på engelska.

Cover picture: Silica optical fiber, used for high-power laser light delivery for the ablation of hard material, such as bone. The fiber is made at Acreo's Fiberlab in Hudiksvall.

Printed by Universitetsservice US AB, Stockholm 2014

Aziza Sudirman

Increased Functionality of Optical Fibers for Life-Science Applications

Department of Applied Physics, KTH – Royal Institute of Technology
106 91 Stockholm, Sweden

ISBN 978-91-7595-122-5, TRITA-FYS 2014:15, ISSN 0280-316X, ISRN KTH/FYS/--14:15—SE

Abstract

The objective of this thesis work is to increase the functionality of optical fibers for possible applications in life-sciences. Optical fibers are a promising technology for use in biology and medicine. They are low-cost waveguides, flexible and have a small cross-section. They can guide high-power light with low loss in a micrometer core-size. These features make fibers attractive for minimally-invasive, *in-vivo* studies. The backwards guidance of the optical signal allows for real-time monitoring of the distance to the scattering targets and to study the environment through Raman scattering and fluorescence excitation. The longitudinal holes introduced in the fibers can be used, for instance, for delivery of medicine to a specific region of a body. They could even be used for the extraction of species considered interesting for further analysis, for example, studying cells that may be cancer-related.

This thesis deals with four main topics. First, a demonstration is presented of the combination of high-power light guidance for ablation, low-power light reflectometry for positioning, and for liquid retrieval in a single fiber. It was found that in order to exploit the microfluidic possibilities available in optical fibers with holes, one needs to be able to combine fluids and light in a fiber without hindering the low-loss light guidance and the fluid flow. Secondly, one should also be able to couple light into the liquids and back out again. This is the subject of another paper in the present thesis. It was also observed that laser excitation through a fiber for the collection of a low-intensity fluorescence signal was often affected by the luminescence noise created by the primary-coating of the fiber. This problem makes it difficult to measure low light-levels, for example, from single-cells. A third paper in this thesis then describes a novel approach to reduce the luminescence from the polymer coating of the fiber, with the use of a nanometer-thick carbon layer on the cladding surface. Finally, exploiting some of the results described earlier, an optical fiber with longitudinal holes is used for the excitation, identification and for the collection of particles considered being of interest. The excitation light is guided in the fiber, the identification is performed by choosing the fluorescent particles with the appropriate wavelength, and, when a particle of interest is sufficiently near the fiber-tip, the suction system is activated for collection of the particle with good specificity.

It is believed that the work described in this thesis could open the doors for applications in life-sciences and the future use of optical fibers for *in-vivo* studies.

Keywords: Fiberoptics, microstructured fiber, fiber-based optofluidics, laser ablation, microfluidics, reflectometry, fluorescence detection, fiber-based spectroscopy

Sammanfattning

Den funktionalitet optiska fibrer och fibersensorer erbjuder är lovande för olika mättillämpningar inom livsvetenskaperna. Bortsett från att fibrerna är utmärkta ljusledare, är de också mekaniskt flexibla och har en passande och hanterbar storlek. De kan leda ljus med hög effekt/intensitet inuti en central kärna i mikrometerstorlek samtidigt som absorptionen, d.v.s. den optiska förlusten är minimal. Dessa fördelaktiga egenskaper gör att optiska fibersensorer är attraktiva för studier inuti den levande kroppen (*in-vivo*) med minimal skada av den närliggande vävnaden. Den tillbakaledande optiska mätsignalen gör det möjligt för realtidsmätningar baserade på, till exempel, Ramanspridning eller fluorescens. I det föreliggande arbetet har vi bl. a. studerat fibrer med långsgående kanaler (kapillärer) excentriskt placerade relativt kärnan, så kallade "hålfibrer". Dessa longitudinella hål som introducerats i fibern vid tillverkningen kan användas för att, exempelvis, leda ett visst läkemedel till ett specifikt område i kroppen. Samma hål kan även användas för att fånga upp biologiska prover, som exempelvis cancerrelaterade celler, som kan anses vara av intresse för vidare analys.

Den föreliggande avhandlingen behandlar fyra delområden av fiberoptiska sensorer. Först presenteras arbeten där laserablation med högeffektsljus kombineras med positionsmätningar, baserade på lågeffektsreflektometri, samt med uppfångning av en vätska i en och samma optiska hålfiber. Detta är en demonstration av att man med samma komponent kan borra igenom hård vävnad (t.ex. ben) för att sedan kunna fånga upp eller optiskt analysera vätska (t.ex. ryggmärgsvätska) som tränger igenom det öppnade hålet. För att fullt ut kunna utnyttja hålfibers funktionalitet krävs ett smidigt sätt att kunna kombinera ljus och vätskor i en och samma fiber utan att varken påverka ljus- eller vätskeledningen. En detaljerad beskrivning av tillvägagångssättet för denna teknologi ges i avhandlingen. Under arbetets gång upptäcktes även att det guidade laserljuset i fibern, som användes för excitation av fluorescenssignalen, påverkades starkt av bakgrundsbruset från fiberns skyddande akrylatbeläggning. Detta medförde en väsentlig svårighet i att kunna mäta de låga signalnivåerna som härrörde från enstaka biologiska celler. I avhandlingen redogörs för ett nytt sätt att minska detta brus från fiberns inre akrylatbeläggning genom att först belägga fiberns mantelyta med ett tunt lager kolatomer innan appliceringen av akrylatet.

Slutligen, genom att dra nytta av tidigare resultat, presenteras i avhandlingen ett sätt för hur en hålfiberkomponent kan användas för excitation, identifiering och för uppfångning av intressanta partiklar. Excitationsljuset guidas genom fibern, identifieringen sker genom att välja en passande detektionsvåglängd och, när en partikel av intresse är tillräckligt nära fiberändan, aktiveras extraktionspumpen som försiktigt suger in partikeln i fiberhålet.

Arbetet som beskrivs i denna avhandling tror kunna öppna många dörrar för olika tillämpningar inom livsvetenskaperna (Life Sciences) och för framtida studier utförda med optiska fibrer inne i den levande kroppen hos människor, djur, eller växter.

List of publications

This thesis is based on the following peer-review journal papers:

- I. A. Sudirman, G. Björk, and W. Margulis, “Reflectometry, ablation and fluid retrieval using an optical fiber,” *Optics Express*, **18**, 134-140 (2010).
- II. A. Sudirman, L. Norin, and W. Margulis, “Increased sensitivity in fiber-based spectroscopy using carbon-coated fiber,” *Optics Express*, **20**, 28049-28055 (2012).
- III. A. Sudirman and W. Margulis, “All-fiber optofluidic component to combine light and fluid,” *IEEE Photonics Technology Letters*, **26**, 1031-1033 (2014).
- IV. A. Sudirman, M. Stjernström, F. Laurell, and W. Margulis, “A fiber optic system for detection and collection of micrometer-size particles,” to be submitted to *Optics Express* (2014).

Related publications not included in the thesis

- A. A. Sudirman, G. Björk, and W. Margulis, “Combining low-coherence reflectometry, laser ablation and fluid collection in a fiber,” Northern Optics Conference, Vilnius, Lithuania, Aug 26-28, 2009.
- B. A. Sudirman, G. Björk, and W. Margulis, “Combining low-coherence reflectometry, laser ablation and microfluidics in a fiber,” 3rd EOS Topical Meeting on Optical Microsystems (OμS09), Capri, Italy, September 27-30, 2009.
- C. A. Sudirman, M. Stjernström, F. Laurell, and W. Margulis, “Single-fiber for minimally-invasive identification and collection of biological species,” Conference on Lasers and Electro-Optics (CLEO), San Jose, USA, May 6-11, 2012.
- D. A. Sudirman and W. Margulis, “Fully spliced optofluidic fiber arrangement,” Workshop on Specialty Optical Fibers (WSOF), Sigtuna, Sweden, Aug 23-26, 2013.
- E. R. M. Gerosa, A. Sudirman, L. de S. Menezes, C. J. S. de Matos, and W. Margulis, “All-fiber high-flow microfluidic dye laser,” Workshop on Specialty Optical Fibers (WSOF), Sigtuna, Sweden, Aug 23-26, 2013.

Description of author contribution

My contribution to the original papers was the following:

Paper I

My co-supervisor, Walter Margulis and I designed the experiments and I performed the experimental work. The paper was written with the assistance of my supervisors: Gunnar Björk and Walter Margulis.

Paper II

My co-supervisor, Walter Margulis and I took part in the design of the experiment and I performed the experiments. The paper was written with the assistance of the co-authors: Lars Norin and Walter Margulis.

Paper III

My co-supervisor, Walter Margulis and I designed the experiments. I performed the experimental work and the paper was written with the assistance of the co-author: Walter Margulis.

Paper IV

Mårten Stjernström and I designed and performed the experimental work. The paper was written with the assistance of the co-authors: Fredrik Laurell and Walter Margulis.

Acknowledgements

There are so many people I would like to acknowledge. To write down everything I would like to say to each and every one of you would, in fact, result in a thesis by itself. So, to keep this as short as possible (but still very sincere) I would like to start by thanking my supervisors: Prof. Gunnar Björk and Prof. Walter Margulis.

Thank you, Gunnar for all of your help, support and words of wisdom during these past five years. It has been a pleasure to have had you as a supervisor. Thank you for giving me the freedom to explore the world of optics. And thank you, Walter for introducing me to the world of research. Since my very first day at Acreo Swedish ICT, you have been my mentor and advisor. I'm very grateful to have been given the opportunity to work alongside such a brilliant scientist.

Thank you, Prof. Fredrik Laurell for taking me under your wing, even though I technically was not one of your Ph.D. students. Thank you for the time and energy you invested in me, and for making me feel included in the Laser Physics group. Thank you for reminding me that there is, in fact, a life after the Ph.D. studies, for preparing me for that life, and for helping me to take the next step in my career. Thank you, Jens Tellefsen for all of your support and help when it came to my thesis writing. Thank you to everyone in the Laser Physics group (and also to the former students) for always making me feel so welcome and part of the Laser Physics family. You guys are wonderful!

Thank you to all of the fantastic people working (and have worked) at Acreo Swedish ICT, the Fiber Optics group (Alexandre, Anna Chiara, Bertrand, Björn H, Carola, Daniel, Erik, Hülya, Magnus, Micke, Ola, Patrik, Paula, Pierre-Yves, Pär, Ralf, Sasha, Sebastian, Walter, and Zhangwei), the super fun Netlab people, Leif Kjellberg and everyone in the Fiberlab in Hudiksvall (Helena, Håkan, Lars, Mats, Niclas, Per, Åsa C, and Åsa S). Thank you all for giving me five years of your lives.

Thank you, my QEO group (Anna Chiara, Amin, Christian, Gunnar, Jakob, Jonas A, Jonas, Katarina, Katia, Marcin, Martin, Matthias, Mauritz, Michele, and Saroosh), and remember that when it comes to Pecha-Kucha presentations – we rock!

Thank you, Prof. Christiano de Matos and all of your students at the Universidade Presbiteriana Mackenzie in São Paulo, Brazil. Thank you for taking care of me during my visit to your Optics and Photonics group and for making me feel so welcome during my stay in Brazil.

Thank you, my amazing ADOPT Ladies (Anna, Anna Chiara, Carlota, Charlotte, Elena, Hoda, Isabelle, Katarina, Kate, Katia, Mahtab, Reyhaneh, Saroosh, Shagufta and Zhangwei), you girls are truly wonderful. Thank you for the lunches and for the therapy sessions throughout the years. A special thank you to Åsa Claesson (Acreo Swedish ICT) and Elizabeth Illy (Cobolt) for attending our ADOPT female lunches. The optics and photonics society in Sweden needs more successful and strong women like both of you, who truly are an inspiration to all of the female students/researchers working in optics and photonics.

Thank you, my partners in crime: Anna Chiara Brunetti and Alexandre de Resende Camara. Thank you, my dear Chiara for being the wonderful person that you are and for being a good friend. You know that the two of us make an awesome team. Together we can (and will) accomplish great things. One brain, remember! And thank you, amazing Alexandre, “King of Acreo”, for always making me laugh so hard that my cheeks actually hurt. You are such a loyal friend with a good and honest heart. Thank you so much for caring about me.

Thank you to all of my friends, for putting up with me during the years of my Ph.D. studies and for understanding that free time was a luxury I could not really afford. Each and every one of you helped me get through these years. And thank you, my two most awesome girls: Rusul Al-Mousavi and Marta Inanoglu. You girls surely have made my life an adventure. Thank you for always being there for me and for holding my hand during the times when life’s challenges have been so overwhelming.

Last but not least, thank you to my wonderful Ibu and Ayah. I know that our family has gone through some tough times during these past five years. But thank you for being patient with me and for understanding that this has not been an easy time for me. Thank you for all of your love and support.

To be really honest, these past five years have been so challenging for me. I have experienced some very joyful moments during my Ph.D. studies, but also some very sad and devastating ones (the top two being when Mårten Stjernström passed away and when my four-year long relationship ended). But I have learned so much during this time, not only about optics and physics, but also a great deal about myself, about my strengths and my weaknesses. I have learned that it is important to surround yourself with honest, kind and loyal people. They will help you get through the tough times. I have been lucky to have met some really amazing people throughout this journey and I am very happy to have them in my life.

I must say that I am quite proud of myself for coming this far, for finishing, and for not giving up. There have been times when I have wanted to throw in the towel. But instead, I chose to work even harder. My thesis is the result of the hard work, the long hours and the many tears I have spent during these five years, and I can, with confidence, say that I am defending this work with pride.

To conclude, I would like to say that surviving Ph.D. studies is not all about having the brains and being smart, but it is equally important to stay focused and determined. I have learned that if you really want something in life you have to work hard for it, and that is exactly what I have been doing, every single day, for the past five years. I wanted this Ph.D. – and I got it!

Contents

Abstract	iv
Sammanfattning	v
List of publications	vii
Related publications not included in the thesis	vii
Description of author contribution	viii
Acknowledgements	ix
Contents	xi
Chapter 1 – Introduction	1
1.1 Optical Fibers for Applications in Life-Science	1
1.2 Motivation of the Thesis Work	2
1.3 Outline of the Thesis	2
Chapter 2 – Basic Theory	3
2.1 Optical Fibers	3
2.2 Fiber Processing	7
2.3 Microfluidics	8
2.4 Reflectometry	11
2.5 Laser Ablation	12
2.6 Optical Detection Methods	13
Chapter 3 – Reflectometry, Ablation and Microfluidics in Fiber	17
3.1 Motivation and Aim	17
3.2 Preliminary Studies	18
3.3 Experiments and Results	22
3.4 Discussion	25
Chapter 4 – Carbon-Coated Fiber for Fiber-Based Spectroscopy	27
4.1 Motivation and Aim	27
4.2 Preliminary Studies	28
4.3 Experiments and Results	32
4.4 Discussion	33
Chapter 5 – Fiber-Based Optofluidic Components	35
5.1 Motivation and Aim	35
5.2 Various Fiber Arrangements	36
5.3 Fully-Spliced All-Fiber Component	40
5.4 Discussion	41
Chapter 6 – Detection and Isolation of Micrometer Particles in Fiber	43
6.1 Motivation and Aim	43
6.2 Preliminary Studies	44
6.3 Experiments and Results	51
6.4 Discussion	54

Chapter 7 – Conclusions	55
7.1 Summary	55
7.2 Outlook.....	56
References.....	57

Chapter 1

Introduction

*Obstacles don't have to stop you.
If you run into a wall, don't turn around and give up.
Figure out how to climb it, go through it, or work around it.*
- **Michael Jordan**

1.1 Optical Fibers for Applications in Life-Science

Silica optical fibers have earlier mainly been exploited in the telecom industry [1]. But, optical fibers have also found applications in areas such as medicine, used in, for instance, minimally-invasive surgery [2], imaging based on optical coherence tomography (OCT) [3,4], and the sensing of various physical parameters such as pressure [5,6] and temperature [6]. The introduction of longitudinal holes in the cladding of the optical fiber multiplies the degrees of freedom available. The holes can be used, for example, for the delivery of medicine to a specific region. They could even be employed for the collection and retrieval of species considered interesting for further analysis.

In order to exploit the microfluidic possibilities available in optical fibers with holes, one needs to be able to combine the light and the fluids in the same fiber without hindering the light guidance and the fluid flow. Optical fibers are a promising technology for single-cell analysis, since they can guide light with low loss in a micrometer core-size and allow for delivery of small fluid volumes. The backwards guidance of the optical signal allows for real-time monitoring of the distance to the scattering targets and, further more, to study the environment through, for instance, Raman scattering or fluorescence excitation. These features make optical fibers attractive even for single-cell analysis.

1.2 Motivation of the Thesis Work

In the last decade the development and the production of microdevices, for instance, lab-on-a-chip devices, have increased tremendously. These devices can be used for detection and analysis of single-cells. These microdevices have been found to be advantageous in the sense that they offer rapid analysis with high sensitivity and that they only require minute sample volumes. Optical fibers can, unfortunately, not offer the same complexity as the lab-on-a-chip devices. However, fibers can be made very long and their small cross-sections make it possible to exploit them for minimally-invasive, *in-vivo* measurements [7]. Optical fibers can also be combined with, e.g., laser technology, which allows one to deliver the laser light to non-transparent and inaccessible locations in the human body [8].

The objective of this thesis work is to increase the functionality of optical fibers for possible applications in life-sciences. It is believed that the work described in this thesis could open the doors for the future use of optical fibers in *in-vivo* studies.

1.3 Outline of the Thesis

This thesis contains a summary of Papers I-IV (found in the back of the thesis) and additional work that was not included in the papers. Chapter 2, introduces the theory necessary for understanding the work done in the four papers, such as the guiding principle of optical fibers, various types of fibers used in the present work, microfluidics (included in Papers I and IV), optofluidics (included in Paper III) and some optical detection methods, such as Raman detection (included in Paper II) and laser-induced fluorescence detection (included in Paper IV). A short introduction to reflectometry and laser ablation (both included in Paper I) is also given.

Paper I is summarized in Chapter 3, where reflectometry, laser ablation, and microfluidics are combined in an optical fiber with longitudinal holes. Chapter 4 discusses the function of carbon-coated fibers for eliminating the luminescence from the polymer coating of the fiber and, thus, reducing the background radiation for applications in fiber-based spectroscopy. Various fiber arrangements for microfluidic applications and an all-fiber optofluidic component are discussed in Chapter 5. Paper IV is summarized in Chapter 6, which includes work done on the isolation of micrometer-sized fluorescent beads using laser-induced fluorescence detection inside of the fiber. Conclusions of the thesis work and outlook for future work are given in Chapter 7.

Chapter 2

Basic Theory

*Nothing in life is to be feared, it is only to be understood.
Now is the time to understand more, so that we may fear less.*
- **Marie Curie**

2.1 Optical Fibers

Optical fibers are well-known for their excellent waveguiding properties. Since their introduction, optical fibers have truly influenced the telecom industry and the way we communicate today [9]. In 2009, Charles K. Kao received the Nobel Prize for his work done together with George A. Hockham suggesting that if the attenuation in optical fibers is reduced to less than 20 dB/km, then long distance propagation would indeed be possible [10]. Now, improved techniques have even made it possible to reduce the fiber attenuation down to 0.2 dB/km.

The standard telecom fibers (STFs) exploited today, are based on fused or synthetic silica and, typically, have a germanium-doped core. These fibers are in general 125 μm in diameter and have an 8 μm diameter core. Introducing, for instance, germanium dopants in the silica glass increases its refractive index. Thus, having a high-index germanium-doped core with a surrounding silica glass cladding will propagate the light in the core through total internal reflection (TIR). Fig. 2.1 is a schematic illustration of how the incoming light is guided in the core through TIR. Here, n_0 is the refractive index of the surrounding media of the fiber, n_{core} and $n_{cladding}$ are the refractive indices of the fiber core and cladding, respectively. θ_0 is the incident light angle and θ_i is the internal reflection angle.

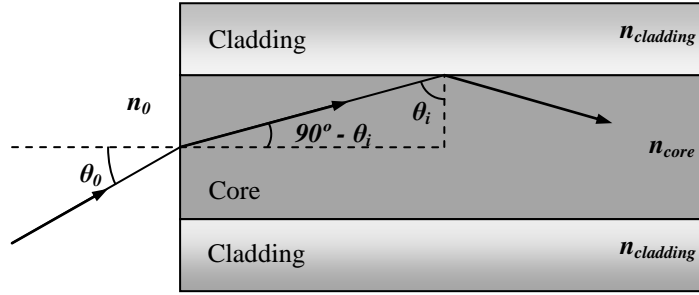


Fig. 2.1 Schematic illustration of light guidance by total internal reflection in an optical fiber.

In order to guarantee guidance of the light by TIR along the fiber, the refractive index criteria, $n_{core} > n_{cladding}$ should be met. But, also, θ_0 should be within the angle given by the fiber's numerical aperture (NA), which is described as the light acceptance angle. From Snell's law of refraction (found in any standard optics textbook [11]), together with the fiber geometry, seen in Fig. 2.1, the fiber NA can be described by Eq. (2.1). For a single-mode standard telecom fiber (SMF28) the NA is typically 0.12-0.14 [12], which translates into a light incidence angle of about 15° .

$$NA = n_0 \sin \theta_0 = \sqrt{n_1^2 - n_2^2}. \quad (2.1)$$

A schematic illustration of a fiber cross-section is seen in Fig. 2.2 (a) below. The refractive index profile of the fiber core and cladding is illustrated in Fig. 2.2 (b). The Gaussian shaped electric field distribution of the fundamental mode of the light in the fiber is seen in Fig. 2.2 (c). The electric field extends beyond the fiber core, but decreases quite rapidly in the cladding region. The part of the field that is in the fiber cladding is referred to as the evanescent field.

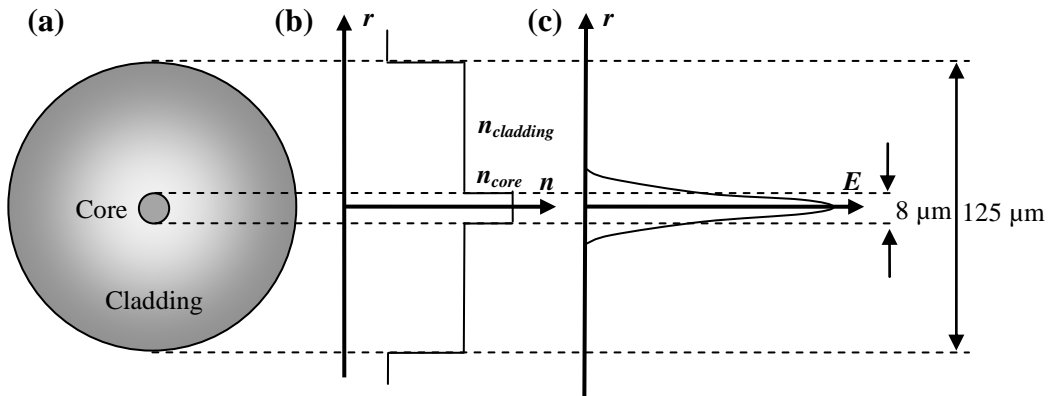


Fig. 2.2 (a) Schematic illustration of a standard telecom fiber cross-section, (b) the refractive index profile in the core and cladding regions, and (c) the electric field distribution of the fundamental mode guided in the fiber.

2.1.1 Microstructured Fibers and Capillaries

The silica microstructured fibers used in the present work are similar to the STFs in terms of the outer-diameter, core-size and the fiber *NA*. But, microstructured fibers have longitudinal holes in the cladding, as seen in Fig. 2.3 below. These microstructured fibers are made by mechanically drilling the holes in the glass preform before the fiber drawing process. The fibers often have multiple side-holes with hole-diameters of typically 20-30 μm . However, the distance between the core and the side-hole can differ, as seen in Fig. 2.3.

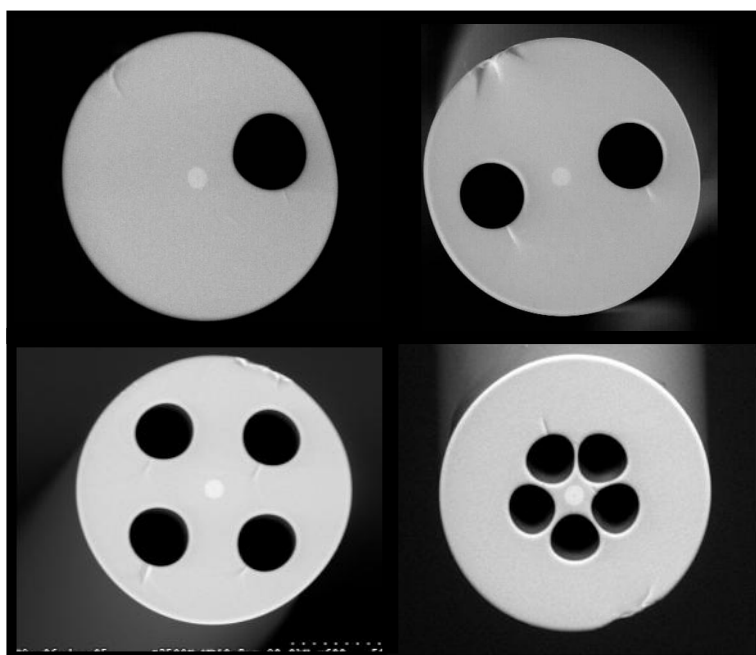


Fig. 2.3 SEM-images of various 125 μm outer-diameter microstructured fibers used in the thesis work. These fibers have an 8 μm core and can either have one (top left), two (top right), four (bottom left), or five (bottom right) side-holes.

Silica fiber capillaries are different from the STFs in the sense that they do not have a waveguiding core, as seen in Fig. 2.4 below. However, if the capillary hole is filled with a high-index material, even the capillaries can be exploited as a waveguide as was demonstrated by J. Stone in 1972 [13]. Capillaries have been exploited for biological analysis, for instance, in capillary electrophoresis since the early 1970s. One of the main advantages of using capillaries is that they allow for small-volume flow-rates, which results in sampling volumes in the picoliter range [14].

Optical fibers are used to an increasing extent in optofluidics [15,16]. A more detailed introduction to fiber-based optofluidics is given in Section 2.3.1. By filling the fiber holes with various materials, the fiber can be employed, for instance, for tuning [17], switching [18], and nonlinear optics [19,20]. We want to point out that the so-called photonic crystal fibers (PCFs) are also widely exploited in fiber-based optofluidics [21,22]. However, this thesis does not include work performed with such PCFs.

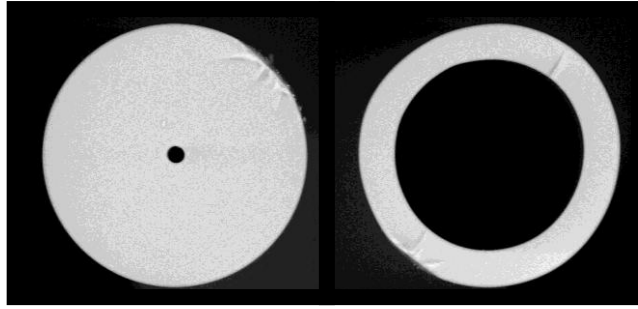


Fig. 2.4 SEM images of a couple of 125 μm outer-diameter silica capillaries used in the thesis work. These capillaries have an inner-diameter of 8 μm (left) and of $\sim 90 \mu\text{m}$ (right), respectively.

2.1.2 Carbon-Coated Fibers

Carbon-coated optical fibers have been developed mainly to be applied in harsh environments [23,24,7]. These fibers are similar to STFs but have a few nanometer thick layer of carbon on the cladding surface. They can be used for sensing in, for instance, oil wells, for aerospace use and for applications undersea. The carbon is deposited on the cladding surface by chemical vapor-deposition (CVD) from a hydrocarbon gas during the fiber drawing process. The carbon layer is $\sim 20 \text{ nm}$ thick and gives the fiber a dark color, as seen in Fig. 2.5 below. The main purpose of the carbon is to prevent the hydrogen and water molecules from diffusing into the fiber. Hydrogen diffusion into the fiber core induces optical loss [25], while moisture accelerates crack growth on the glass surface [26].



Fig. 2.5 Image of standard telecom fiber with a $\sim 20 \text{ nm}$ thick carbon-coating.

The broadband absorbance, A_λ , of the carbon-coating is here estimated by illuminating an SMF28 together with a carbon-coated fiber from the side with a HeNe laser. The absorbance is described as $A_\lambda = \ln(P_i/P_{transm})$. The transmission through the carbon-layer at 633 nm wavelength is 75%, meaning that the carbon-coated fibers used here for visible wavelengths has an absorbance of $A_{\lambda=633nm} = 0.29$.

In Paper II, carbon-coated fibers have been exploited for reducing the luminescence background from the polymer coating of the fiber. In this way, the sensitivity in fiber-based spectroscopy can be increased.

2.2 Fiber Processing

Throughout the thesis work, the fibers and capillaries are processed in various ways. Here, we describe the three main fiber processing methods; splicing, polishing, and etching.

2.2.1 Splicing

When working with optical fibers, it is often required to cleave and re-join them. This process of re-joining fibers is referred to as splicing. This is done using a splicer machine, for example, of type Ericsson FSU 995 PM Fiber Optic Splicer. The fibers are cut with a special fiber cleaver and placed in the holders of the splicing machine, which then melts the two fiber ends together, after aligning them so the position of the fiber cores match up. A fusion splice between two STFs typically results in an optical loss of < 0.1 dB.

2.2.2 Polishing

The side-holes of a microstructured fiber, or the hole of a capillary, can be accessed from the side by polishing. The setup for polishing is shown in the photograph in Fig. 2.6. The fiber/capillary is fixed on a glass slide, for instance, using tape, and then placed under a microscope, which is employed for visualization of the polishing process. Next, a rotating drum with an attached mesh (polishing) paper is brought towards the fiber/capillary.

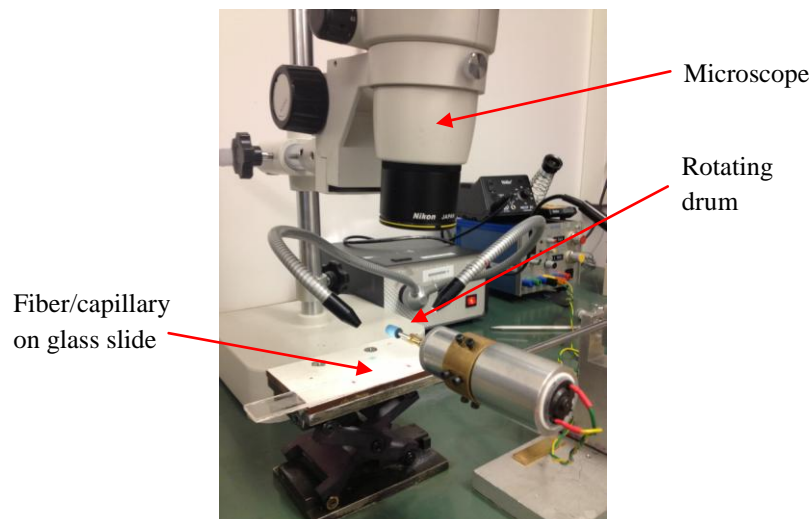


Fig. 2.6 Image of the fiber polishing setup. The fiber is fixed on a glass slide and the polishing is done (under the microscope) by bringing the rotating drum towards the fiber.

The polishing time for opening a side-hole of a microstructured fiber or a capillary hole is roughly a few seconds. But, the exact polishing time depends on the amount of glass that needs to be removed. The polishing is stopped when an opening on the side of the fiber has appeared. A polished opening is ~ 1 mm long. In order to minimize the amount of glass debris entering the side-hole/capillary hole during the polishing, a ~ 20 μm thin metal wire is inserted into the fiber side-hole/capillary hole from the fiber/capillary end. The wire is removed after the polishing is finished. If a thicker capillary is to be polished, for instance, a 250 μm outer-diameter capillary with 127 μm inner-diameter (used in the work in Paper III), a standard 125 μm fiber can be inserted into the capillary hole to prevent glass debris from entering the hole.

2.2.3 Etching

In the present work, etching of the outer-diameter of the fiber has sometimes been necessary. For this purpose, hydrofluoric acid (HF) with a concentration of 40-50% is used. The etching is done by simply immersing the fiber directly in the HF, which etches the fiber isotropically. The etching rate of silica for this concentration of HF is ~ 1 $\mu\text{m}/\text{min}$. The etching rate of the fiber core is higher than that of the silica, so if a flat endface is needed, the cleaving of the fiber tip should take place after the etching process. It is found difficult to etch small holes from the inside, for instance when one wants to fit a fiber inside a capillary. It is then preferred to use a capillary with a larger inner-diameter to start with. The polymer-coating is not perfectly impermeable to HF. Therefore, when etching a silica fiber, the polymer primary-coating should first be removed to ensure that the entire section of the fiber to be etched is exposed to the HF.

2.3 Microfluidics

Microfluidics is the science and technology of fluid manipulation on the micrometer scale [27]. Here, the term fluids typically include both liquids and gases. Microfluidic devices allows for handling of very small sample volumes and with short reaction times. Another advantage of downscaling to micrometer-size devices is the increase of the surface-to-volume ratio, which can be beneficial, for instance, in capillary electrophoresis where the excess heat is removed more rapidly. Microfluidics usually is exploited in lab-on-a-chip technology and in other microdevices for various applications in life-sciences [28].

The physics of microfluidics can be explained by the Navier-Stokes, equation, Eq. (2.2), which can be found in standard physics text books [29]. The Navier-Stokes equation is obtained when applying Newton's second law to fluid motion. The parameter \mathbf{u} is the fluid flow speed, ρ is the fluid density, p is the pressure and η is the fluid viscosity. Seen in Eq. (2.2), $\rho(\mathbf{u} \cdot \nabla \mathbf{u})$ is defined as the net fluid flow

momentum, and $\rho(\partial\mathbf{u}/\partial t)$ is the temporal change in the fluid momentum. Here, the law of mass and the energy conservation (for a compressible fluid) should be taken into consideration, meaning that $\nabla\rho\mathbf{u} = 0$. The pressure and the viscous forces are expressed as ∇p and $\eta\nabla^2\mathbf{u}$, respectively, and the body forces acting on the fluid are described by \mathbf{f} , as seen in Eq. (2.2). In this form, the Navier-Stokes equation can be written in the following way:

$$\rho\left(\frac{\partial\mathbf{u}}{\partial t} + \mathbf{u} \cdot \nabla\mathbf{u}\right) = -\nabla p + \eta\nabla^2\mathbf{u} + \mathbf{f}. \quad (2.2)$$

Another parameter that is frequently mentioned when it comes to microfluidics is the Reynolds number, Re , which describes the ratio between the inertial and the viscous forces. The derivation of Re can be found in the paper by Squires and Quake [30]. The Reynolds number is defined as:

$$Re = \frac{\rho U_0 D_h}{\eta}. \quad (2.3)$$

In Eq. (2.3), U_0 is the mean velocity of the fluid and D_h is the hydraulic diameter, defined as $D_h \equiv 4A_{cross}/P_{wet}$, where A_{cross} is the cross-section area and P_{wet} is the perimeter of the channel walls that are in contact with the fluid. When Re is very small, which is usually the case when dealing with microfluidics, it means that the viscous forces dominate the fluid behavior. The inertial forces become, in that case, irrelevant. A small Reynolds number also tells us that the nonlinear terms ($\mathbf{u} \cdot \nabla\mathbf{u}$) in Eq. (2.2) can be neglected, resulting in a linear and predictable Stokes flow. For the case of $Re < 2300$, the flow is considered laminar. When Re is approaching the value of 2300, the fluid starts showing signs of turbulence [31]. A laminar fluid in a pipe (or capillary) has a typical behavior as shown in Fig. 2.7, where the fluid-flow speed is illustrated with the arrows and has its maximum in the center of the pipe (or capillary).

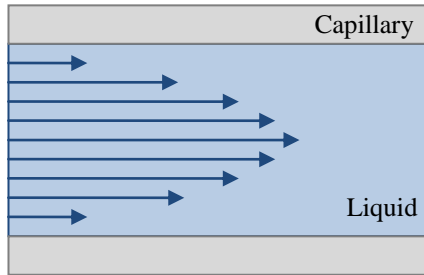


Fig. 2.7 Schematic illustration of the flow profile of a laminar liquid inside a micrometer-sized capillary. The flow speed is at its maximum in the center of the capillary.

For the calculation of the flow properties, such as the volumetric flow rate, Q , in a capillary, the equation of Hagen-Poiseuille is used, as shown in Eq. (2.4) below. Here, ΔP is the absolute value of the pressure difference between the pressure *inside* the capillary and the pressure at the capillary end, r_{cap} is the radius of the capillary's

inner-diameter, η is the fluid viscosity and L_{cap} is the length of the capillary. The Hagen-Poiseuille flow formula is also derived by the Navier-Stokes formula [32]. The parameter, R_{fluid} , in Eq. (2.4) is described as the fluidic resistance. The Hagen-Poiseuille equation is given by:

$$Q = \frac{\Delta P \pi r_{cap}^4}{8\eta L_{cap}} = \frac{\Delta P}{R_{fluid}}. \quad (2.4)$$

The control and manipulation of the fluid flow in capillaries can be performed with, for instance, the applied pressure difference, the applied electric fields, or the capillary forces [33]. In the present work, the fluid is only controlled using the applied pressure difference (as described in Papers III and IV). However, in Paper I, there are no external forces applied in the fluid handling; capillary action alone influenced the fluid, when the fluid was collected inside the side-holes of the fiber.

The capillary height, H , of the fluid collected inside the capillary hole can be estimated using Eq. (2.5) as derived from the Young-Laplace equation for the pressure drop across a curved interface [32]. Here, g is the gravitational acceleration, d_{cap} is the capillary hole-diameter, ρ is the fluid density, γ_{sg} is the surface tension between the solid and the gas and γ_{sl} is the corresponding surface tension between the solid and the liquid phase. The height, thus, can be expressed as follows:

$$H = \frac{4}{\rho g d_{cap}} (\gamma_{sg} - \gamma_{sl}). \quad (2.5)$$

In the thesis work, microfluidic considerations have been included in Papers I, III and IV. However, when combining optics and microfluidics, as for instance in the case of our microstructured fibers and/or capillaries, a new field is introduced – *optofluidics*.

2.3.1 Optofluidics

Optofluidics combines optics with microfluidics [34,15]. Optofluidics has mostly been associated with planar waveguide structures. But recent developments in fiber-based optofluidics clearly show that optical fibers also offer a promising platform for optofluidics [35,15,16]. The use of fibers in optofluidics offers some advantages over planar geometries in two aspects. On one hand, very long devices can be exploited for enhanced resolution, as for example in capillary electrophoresis [36]. On the other hand, the minute cross-section available in fibers makes them ideal for *in-vivo* measurements, e.g., in minimally-invasive diagnostics [7], pressure sensing in the body [5], and 3D imaging with fiber optical coherence tomography [3].

In order to exploit the microfluidic possibilities available in fibers with holes, one needs to be able to combine the light and the fluids in the same fiber without hindering the light guidance and the fluid flow. In the present work, an all-fiber arrangement for combining light and small-volume fluid delivery is described

(discussed in Paper III). These fully-spliced fiber arrangements offer more user-friendly components, for instance, for future clinical use in single-cell analysis, without utilizing non-ideal bulky cells for free-space coupling of light and pumps for fluid filling in components with a large dead-volume.

2.4 Reflectometry

Low-coherence reflectometry is a quasi-coherent detection technique based on Michelson interferometry [37]. A simple schematic illustration of the low-light reflectometry principle is given in Fig. 2.8 below. The signal from the short coherent-length LED-source is split into two parts; a reference arm and a signal arm. The latter arm also includes an additional optical fiber part with the fiber-tip acting as a probe. The reflected light is then guided back via the fiber. The optical delay for the reflected light in the reference arm is controlled by the translation of a movable mirror (actually a retroprism). If the optical delay of the reflected reference matches the delay of the returning reflected light in the signal arm, interference in the detector plane occurs. However, this will only happen if the optical distance to the reference mirror is within a coherence length as compared to the optical distance of the signal arm. The interference signal reaches the detector and strips away unwanted fringes. The signal is proportional to the square root of the optical reflectivity, which is then squared and displayed as a function of the mirror position.

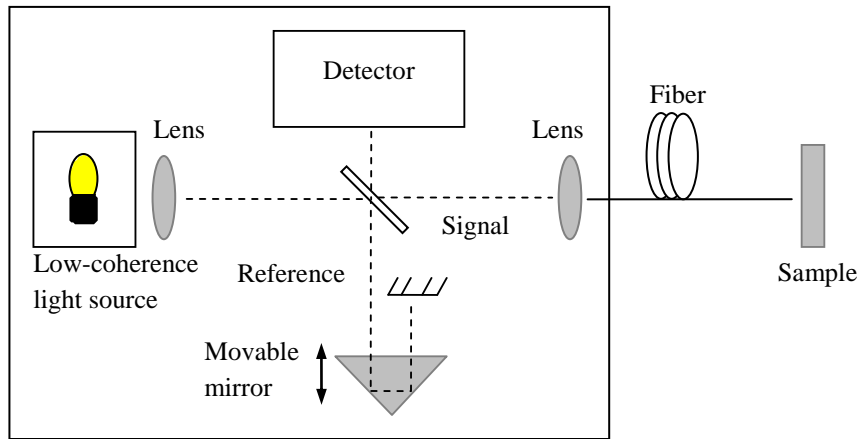


Fig. 2.8 Schematic illustration of low-light reflectometry. The part inside the square shows the Michelson interferometer. The signal from the LED light source is coupled to an optical fiber used for probing reflection surfaces.

The reflectance, R_{12} , obtained when the light travels, for example, from gas to solid, can be estimated with the help of Fresnel's equation, shown below in Eq. (2.6). Here, n_1 and n_2 are the refractive indices of the two media, respectively. The derivation of this equation can be found in standard optics text-books [38]. For air/water and air/glass interfaces, the reflectances are typically $\sim 2\%$ and $\sim 4\%$, respectively. For a water/glass interface the reflectance is a mere 0.2% . The

amplitude difference, A_{12} , in dB can then be estimated by Eq. (2.7), where R_1 is the reflectance in air and R_2 is the reflectance due to index-matching. In Paper I, Eq. (2.7) is applied when estimating the amplitude change of the fiber-tip when being inserted in different media. For normal incidence, the reflectance and the amplitude difference are given by:

$$R_{12} = \left(\frac{n_1 - n_2}{n_1 + n_2} \right)^2, \quad (2.6)$$

$$A_{12} = 10 \log \left(\frac{R_1}{R_2} \right). \quad (2.7)$$

2.5 Laser Ablation

Laser ablation involves the removal of material using laser light [39]. This common method is applied in various fields for removal and cutting of, for instance, metals, dielectric materials such as glasses and plastics, and biological materials. Laser ablation can be performed with either pulsed or continuous wave laser light [40,41]. The ablation experiments described in Paper I were performed with pulsed laser light. The pulsed laser-ablation mechanism is defined by the following parameters; the material absorption wavelength, the laser pulse duration, the pulse repetition rate, the pulse energy and the laser beam diameter. These five irradiation parameters influence the ablation process in various ways. The laser wavelength determines the material absorption and the scattering coefficients. The pulse duration determines the rate of laser energy deposition. The pulse repetition rate defines whether heat accumulation effects have to be considered. Finally, the laser pulse energy determines the total amount of heat generated in the focal region and the beam diameter determines the effective radiation fluence.

The pulse intensity, I_{pulse} , as measured in W/unit area, can be described as $I_{pulse} = E_{pulse}/(\tau_{pulse}A_{eff})$. Here, A_{eff} is the effective area of the laser beam, with a $1/e^2$ beam diameter (assuming that the beam has a Gaussian beam shape profile). τ_{pulse} is defined as the pulse duration. The pulse energy, E_{pulse} , can then be estimated from the laser-pulse peak power, P_{peak} , and the pulse duration by the relation, $E_{pulse} = P_{peak}\tau_{pulse}$. The total energy is expressed as E_{pulse} multiplied with the number of laser pulses. With this approximate relation, the effective fluence (or energy density), Φ_{eff} , as described in Eq. (2.8), can be determined by:

$$\Phi_{eff} [J/cm^2] = \frac{Total\ energy}{A_{eff}} \quad (2.8)$$

The material absorption of the laser energy can be described by either the linear or the nonlinear processes, whatever is relevant in each case. Linear absorption

is the main absorption mechanism at low intensities and with micro- and nanosecond pulse widths. However, nonlinear absorption can become dominant at high intensity that can mostly be achieved with pico- and femtosecond pulse widths [42]. For micro- and nanosecond laser pulses, the ablation process is dominated by heat conduction, melting, evaporation and plasma formation, as illustrated in Fig. 2.9. During the interaction of these low-intensity pulses with the material, the laser energy is absorbed by free electrons on the surface, which is a process described as the inverse Bremsstrahlung [43]. This, together with the material heat conduction, leads to the formation of a temperature field gradient in the material. Depending on the achieved maximum temperature, the material is either melted, evaporated, or is transferred to a plasma state.

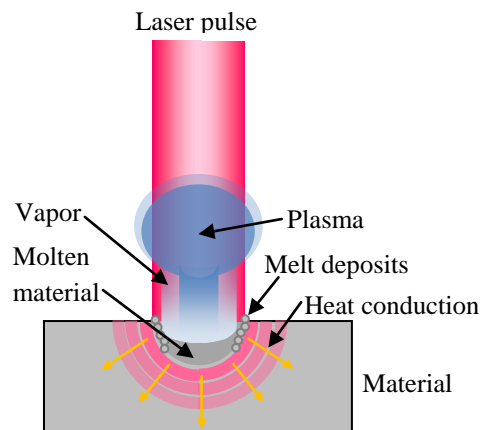


Fig. 2.9 Illustration of the ablation process with low intensity, short laser pulses. The material is exposed to laser irradiation causing it to evaporate, melt, and to be transferred to a plasma state.

Ablation using laser light have been found useful in medicine when it comes to penetrating biological tissues, such as bone [44,45], teeth [46] and even soft tissues [47]. Lasers are therefore used, for instance, in ophthalmology and in surgery. Combining laser technology such as laser ablation, with optical fibers would allow for the laser light to be delivered to non-accessible and non-transparent locations in the human body. This could possibly open up doors for minimally-invasive, *in-vivo* measurements.

2.6 Optical Detection Methods

Detection and analysis at a single-cell level is of importance for preventing the spread of diseases caused by a small number of aggressive cells. One such example is cancer, where the disease progression is determined by the presence of metastatic cells that can spread from the initial tumor and make the disease much more difficult to treat [48]. Another example is the spread of food-borne pathogens, such as bacteria. These pathogens are easily transmittable through food supplies, which can be considered a potential public health problem [49].

Optics has long been used for sensing of biological samples. In recent decades, optical sensing systems have evolved from bulk systems to microdevices [50]. These microdevices enable small-volume sample-handling for performing functions such as particle sorting, counting, and separation, cell culturing and concentration gradient formation. Optical properties, such as the refractive indices, fluorescence spectra, Raman scattering and ditto absorption can be exploited to generate the sensing signal.

In the thesis work, the main focus has been on sensing based on fluorescence excitation and Raman scattering. The Raman signal is typically orders of magnitude weaker than the fluorescence signals [51]. The background signal originating from the laser source, the optical fibers, and all of the optical components can thus easily overwhelm the weak Raman signal. These background signals must therefore be reduced to accomplish sensitive *in-vivo* measurements. In Paper II, a method is suggested for increasing the sensitivity in fiber-based spectroscopy for Raman detection in organic solvents by using carbon-coated fibers.

2.6.1 Laser-Induced Fluorescence

The success of fluorescence detection in life-science applications is partly due to its high sensitivity, but also to the fact that the analysis of species can be performed with a fluorescent tag. Laser-induced fluorescence is a well-known detection method used in microdevices [52], where the fluorescence detection is typically performed using an argon-ion laser with emission wavelength of 488 nm.

In this technique, an attached fluorophore is what causes a molecule to absorb energy at a specific wavelength and then re-emit the energy at a different wavelength. The emitted wavelength depends on the type and the chemical environment of the fluorophore. A more detailed description of the fluorescence emission is shown in the Jablonski diagram in Fig. 2.10 below. A laser source with a specific wavelength is used for the excitation of the fluorophore, which quickly relaxes to the lowest vibrational level of the excited electronic state. This vibrational relaxation process is on the time scale of femtoseconds to picoseconds. The so-called Stokes shift is caused by the difference in energy between the absorbed pump energy and the energy of the photon emitted. Fluorescent emission occurs as the fluorophore decays from the electronic excited state to a vibrational level in the electronic ground state. Fluorescence has typically a lifetime of nanoseconds. Most fluorophores absorb and emit in the wavelength range of 300 to 700 nm [53].

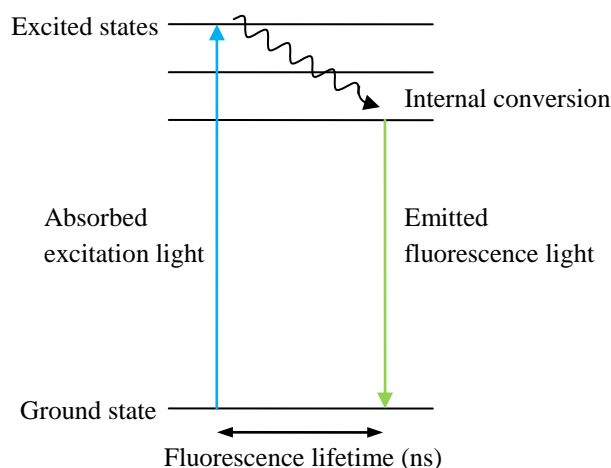


Fig. 2.10 A Jablonski diagram describing the principle of fluorescence light.

When a molecule is exposed to light having an energy that matches an electronic transition within the molecule, some of the light energy will be absorbed as the electron is promoted to a higher energy orbital. But, such an electron excitation preferably occurs from the highest occupied molecular orbital, typically the ground state, to the lowest unoccupied molecular orbital, the excited electronic state. The wavelength absorption band corresponding to the energy difference between two such states (according to the *particle in the box model*) can be described by Eq. (2.9), which is derived from the well-known Schrödinger equation since a molecular orbital can, in fact, be described using the wave property of the electron in the outer shell of a molecule. In Eq. (2.9), ΔE is the energy difference, h is Planck's constant, m_e is the electron mass and L_{box} is the "length" of the molecular box. $n_{excited}$ and n_{ground} are the quantum number of the excited and the ground states, respectively.

The required energy for this electronic transition can thus be provided by a photon with a suitable frequency. This energy can be determined by Planck's relationship, $E = h\nu = hc/\lambda_0$, where ν is the frequency, c is the speed of light in vacuum, and λ_0 is the wavelength in vacuum:

$$\Delta E = \frac{h^2}{8m_e L^2} (n_{excited}^2 - n_{ground}^2). \quad (2.9)$$

2.6.2 Rayleigh and Raman scattering

The scattering of light takes place when an electromagnetic (EM) wave encounters a molecular medium, such as a solid, a liquid, or a gas. As the EM wave interacts with the medium, the electron cloud of the molecules is perturbed with the same frequency as the electric field of the incident wave. The perturbation of the electron cloud results in an induced electric dipole moment, causing scattered light to be emitted at the same frequency as that of the incident light. This scattering process is referred to as *elastic scattering*. An example of elastic scattering is, for instance,

Rayleigh scattering, where the incident and the scattered photons have the same energy. However, the induced dipole moment can also scatter some additional light at other different frequencies, a process referred to as inelastic scattering with the meaning that there is an energy difference between the incident light and the scattered light. Raman scattering is one such example of inelastic scattering, which was discovered by C. V. Raman et al. in 1928 [54]. The energy lost by the incident wave is stored into the medium in the form of vibrational energy, named phonons. The origin of Raman scattering effects resides in the interaction of light with these phonons. In the Raman process, high frequency vibrational states are presented as optical phonons.

The strength of the induced dipole moment, \mathbf{P} , is given by the expression $\mathbf{P} = \alpha\mathbf{E}$, where α is the polarizability and \mathbf{E} is the strength of the electric field of the incident EM wave, which can be expressed as $\mathbf{E} = E_0 \cos(2\pi\nu_0 t)$, where E_0 is the amplitude of the incident wave, ν_0 is the frequency of the wave, and t is the time. The dipole moment can then be expressed as $\mathbf{P} = \alpha E_0 \cos(2\pi\nu_0 t)$. The ability to perturb the electron cloud of a molecule depends on the position of the individual atoms. These atoms are confined to specific vibrational modes, in which the vibrational energy levels are quantized, similar to electronic energies. The vibrational energy of a particular mode is given by Eq. (2.10) below, where j is the vibrational quantum number, ν_{vib} is the vibration frequency and h is Planck's constant:

$$E_{vib} = (j + 1/2)h\nu_{vib}. \quad (2.10)$$

The principle of Raman scattering is shown in Fig. 2.11. The Raman emission can either be such that the scattered photon has less energy (Stokes) or more energy (Anti-Stokes) than that of the incident photon.

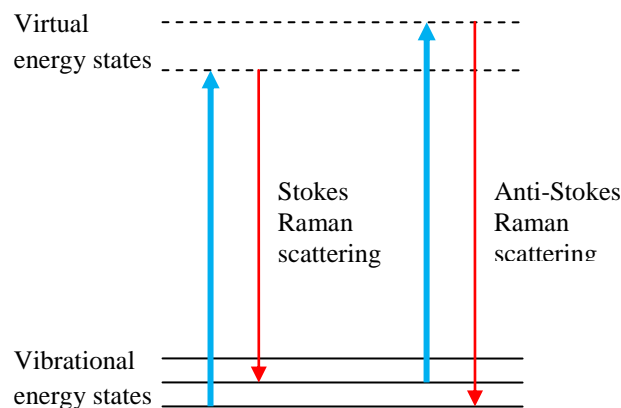


Fig. 2.11 Schematic illustration of Raman scattering, both Stokes shifted and anti-Stokes shifted.

Chapter 3

Reflectometry, Ablation and Microfluidics in Fiber

*Success is not final, failure is not fatal.
It is the courage to continue that counts.*
- **Winston Churchill**

3.1 Motivation and Aim

The objective of this work is partly to develop a method for laser ablation with as little damage of the ablated material as possible. The long-term future aim, however, is to apply this method in life-sciences, for instance, for minimally invasive biopsy, where it is crucial not to damage the surrounding tissue area. Another completely different application would be the study and the collection of liquids in small inclusions trapped in rocks, an application of interest to geologists.

The laser power is delivered through an optical fiber. The positioning of the fiber for ablation is done using optical, low-coherence reflectometry. By exploiting a microstructured fiber with longitudinal holes, collection of the liquid from the ablated region can be accomplished. Both the ablation itself and the liquid collection process can be monitored in real-time using reflectometry. Thus, for this purpose, we combine low-coherence reflectometry, laser ablation, and microfluidics, which is the main objective of the present work.

3.2 Preliminary Studies

3.2.1 Low-Coherence Reflectometry

For the reflectometry experiments in the thesis work, an Ando AQ7410B reflectometer with a short coherence-length LED-source was used. The wavelength of the reflectometer signal was 1310 nm. The nominal spatial resolution of the reflectometer was 20 μm and the detection range was 1.3 m. The sampling resolution was 2 μm and the measurement sweep speed was 36 mm/s [55].

A preliminary study was made on air inclusions in glassy material. These inclusions are formed during the cooling of the glass to the solid phase and can have various sizes. A proper alignment of the setup should minimize the sensitivity of the reflectometer to the surface of the glass surface roughness. For the alignment and the visualization of the inclusions under study, the reflectometer signal and the red light from a HeNe laser were combined, as illustrated in Fig. 3.1. In some of the reflectometry experiments, a 10x microscope objective was used for collimating the beam from the fiber.

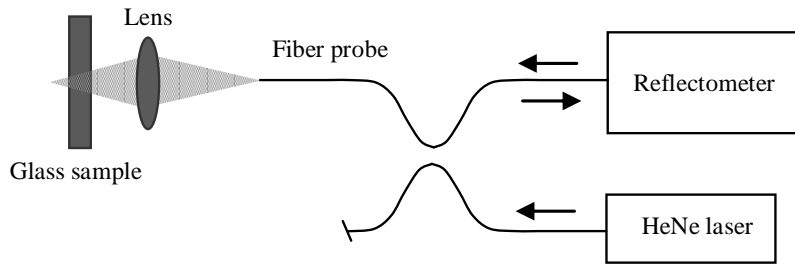


Fig. 3.1 Schematic illustration of the experimental setup of the preliminary low-coherence reflectometer.

The reflectometer signal was guided through the fiber and a specific inclusion in a 0.47 mm thick glass sample was illuminated, resulting in reflection signals at different absolute positions. The two major reflection peaks, seen in Fig. 3.2 below, are from the glass sample's back and front surfaces, respectively. The depth of the inclusion, when assuming that the inclusion was homogenous, is given by the absolute position of the reflections in relation to the glass sample surfaces. The optical distance between the two marked reflection peaks, estimated to be 25 μm in accordance to the scale of Fig. 3.2, illustrates the beginning and end points of the inclusion. When determining the exact inclusion depth, the refractive index of the included material has to be taken into consideration. Assuming for simplicity that the inclusion is air-filled, its depth is determined by using Eq. (3.1) below, an equation derived from Snell's law:

$$d_{sample} = \frac{n_{refl}d_{refl}}{n_{sample}} \quad (3.1)$$

Here, d_{sample} and d_{refl} are defined as the optical distance of the sample and the reflectometer, respectively. n_{sample} and n_{refl} are the refractive indices of the sample and the reflectometer, respectively. The refractive index value of the reflectometer is pre-set to 1.462. The depth of the inclusion is calculated to be 37 μm . Additional experiments of our preliminary study were made with silica fiber capillaries, and these are described in detail in Paper I.

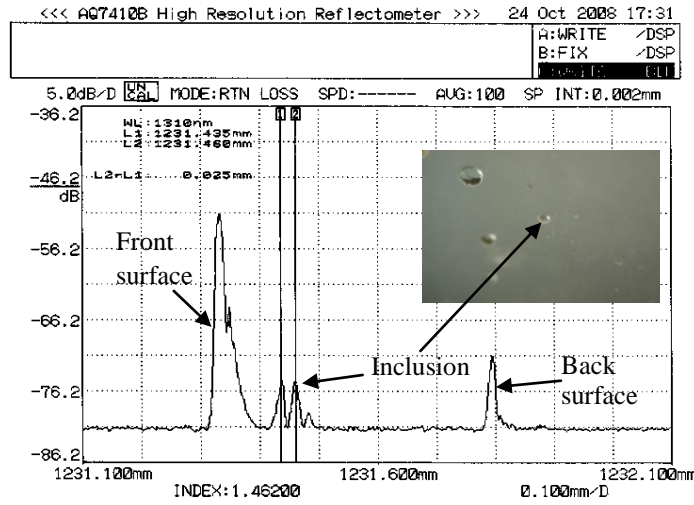


Fig. 3.2 Reflection peaks illustrating the sample thickness and the inclusion depth, with regards to its position in the glass sample.

3.2.2 Fluid Collection in Fiber

Some proof-of-principle microfluidics experiments have been performed, in which the liquid collection in the longitudinal side-holes of a microstructured fiber was monitored using the reflectometer. The microstructured fiber-tip gives a reflected intensity peak of 30 dB above the noise floor. Adding a drop of distilled water on a glass sample and positioning the fiber-tip ~ 1 mm away from the liquid surface would result in a reflected signal from the glass sample together with the liquid surface. The fiber-tip was then brought down towards the liquid surface, as illustrated in Fig. 3.3 (a), (b) and (c), with the corresponding reflectometer traces as shown in Fig. 3.4 (a), (b) and (c), respectively. In Fig. 3.3 (d), the optical distance between the fiber-tip and the liquid surface is < 20 μm , thus the two independent reflections can no longer be distinguished and only one single reflected peak is seen, as shown in Fig. 3.4 (d). As soon as the fiber-tip is in direct contact with the liquid as shown in Fig. 3.4 (e), the reflection amplitude decreases, due to the approximate matching of refractive indices between the optical fiber and the water. The water is then collected via the capillary forces in the side-holes of the fiber, illustrated in Fig. 3.3 (e). The fiber-tip and the

liquid surface reflections reappear, as seen in Fig. 3.4 (f), when the fiber-liquid contact is broken, as shown in Fig. 3.3 (f).

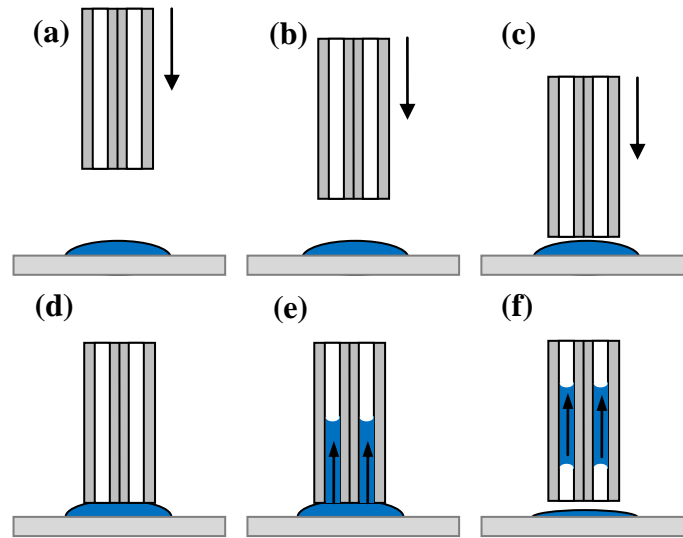


Fig. 3.3 Each step of the liquid collection process that is monitored by the reflectometer.

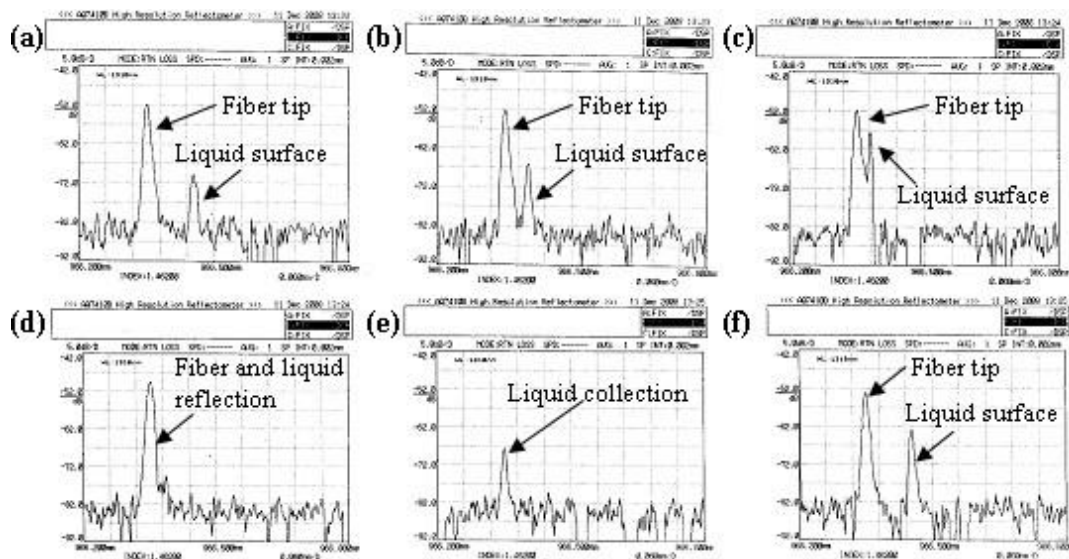


Fig. 3.4 The corresponding reflectometer traces to each of the liquid collection steps shown in Fig. 3.3.

3.2.3 Ablation

For the ablation experiments, a Q-switched and mode-locked Nd:YAG laser was used. It had an operating wavelength of 1064 nm and a repetition rate of up to 4.2 kHz. The peak power of each individual ~ 200 ps pulse was estimated to be 40 kW. Each Q-switched train of pulses contained ~ 100 μ J energy distributed in ~ 20 pulses and with $\sim 30\%$ of the energy contained in the pre-lasing part of the pulse. Using Eq.

(2.8), the effective fluence used for the ablation was calculated to be 0.6 J/cm^2 . According to the literature data [56], this regime of laser operation should result in efficient ablation. A frequency-doubling potassium titanyl phosphate (KTP) crystal was used to generate second-harmonic green light (532 nm), which was in our case mainly used for visualization of the ablation light. It has been reported that the combination of the second harmonic and the fundamental radiation can in, fact, reduce the threshold for ablation [57].

In the present work, since the main objective was to combine the three areas (see Section 3.1) in a proof-of-principle experiment, not so much time was spent in investigating the optimal parameters for ablation using this laser source. The choice of material used for the ablation experiment was based on the relatively low laser power available, the material heat conduction properties, and the amount of debris formed during the ablation. Here, in our investigation, a material with a low heat-conductivity was preferred, since it was desired to only damage the area being exposed to the laser irradiation and not to affect the surrounding area by an increase in the temperature, which could possibly result in the surrounding material being melted. Despite the high heat-conductivity of aluminum, the material chosen for the ablation experiment was a piece of 23- μm thick aluminum foil, which was expected to be an “easy” material to ablate because of its thickness.

The average power of the laser is described as the pulse energy multiplied by the laser repetition rate. An average power of $\sim 300 \text{ mW}$ was sufficient for the ablation of the aluminum foil sample. The maximum average power coupled through the fiber was $\sim 600 \text{ mW}$. The observed ablation time was ~ 1 second. The ablation time could be varied by adjusting the repetition rate. *Decreasing* the repetition rate by a factor of two would *increase* the ablation time with a factor of two. No ablation of the aluminum foil occurred if it was illuminated with less than 500 mW average power when the laser was operated in the continuous-wave (cw) mode. This clearly demonstrates that the ablation process is mainly determined by the intensity of the short pulses, and not by the temperature increase of the sample.

Due to the divergence of the laser beam, the required distance for ablation was $< 1 \text{ mm}$. To avoid damaging the fiber-tip at such a small separation, the distance between the fiber-tip and the sample should be kept $> 50 \mu\text{m}$. Fig. 3.5 (a), (b), and (c) illustrate the ablation process as monitored by the reflectometer. The 17 dB decrease of the aluminum reflection amplitude, seen in Fig. 3.5 (c), clearly illustrate the ablation of the aluminum and the resulting opening of a hole in the aluminum foil.

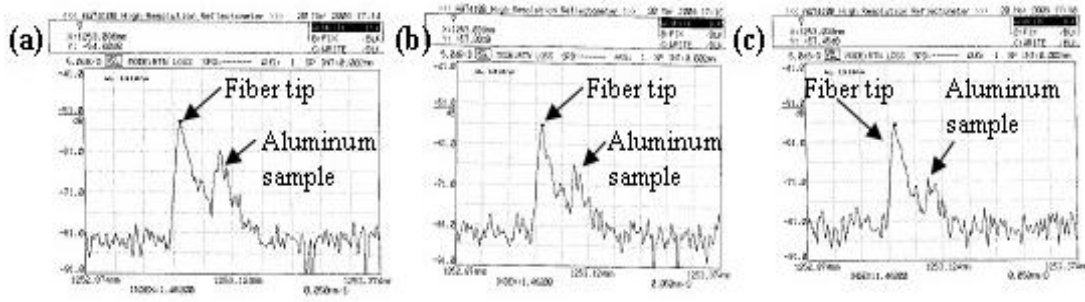


Fig. 3.5 Illustration of the ablation of the aluminum sample as monitored by the reflectometer.

3.3 Experiments and Results

The experimental setup (combining the three studied techniques) is schematically illustrated in Fig. 3.6. For this proof-of-principle experiment, a small plastic container was filled with a Rhodamine 6G dye solution and covered with a piece of aluminum foil to act as a membrane. The dye solution was injected in the container through an opening on the side using a syringe.

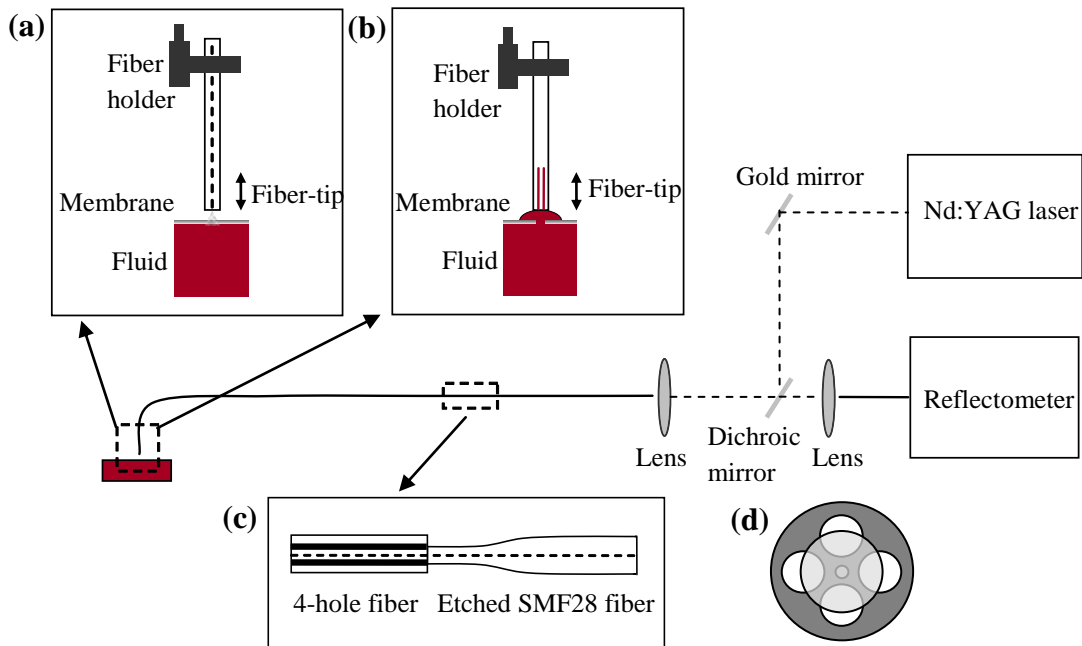


Fig. 3.6 Schematic illustration of the experimental setup, with (a) the positioning of the fiber for ablation and (b) the fluid collection, using (c) the fiber arrangement described in Section 5.2.1. (d) Schematic illustration of the cross-section of the fiber arrangement.

The positioning of the microstructured 4-hole fiber used for the ablation is seen in Fig. 3.6 (a). After a hole through the membrane was ablated, the liquid was sucked up into the fiber side-hole as is illustrated in Fig. 3.6 (b). The ablating laser

light, together with the reflectometer signal, was coupled into the fiber using a non-achromatic 10x microscope objective. The fiber arrangement used here, which is schematically illustrated in Fig. 3.6 (c), consisted of a 125 μm outer-diameter microstructured 4-hole fiber spliced to a piece of standard single-mode telecom fiber (SMF28), where a section of the latter had been etched to $\sim 50 \mu\text{m}$ outer-diameter. The fiber arrangement is further described in Section 5.2.1. Employing such an arrangement allows for a liquid collection using only capillary forces, since the side-holes are not entirely closed when being spliced to the etched SMF28. A cross-section of the fiber arrangement is shown in Fig. 3.6 (d).

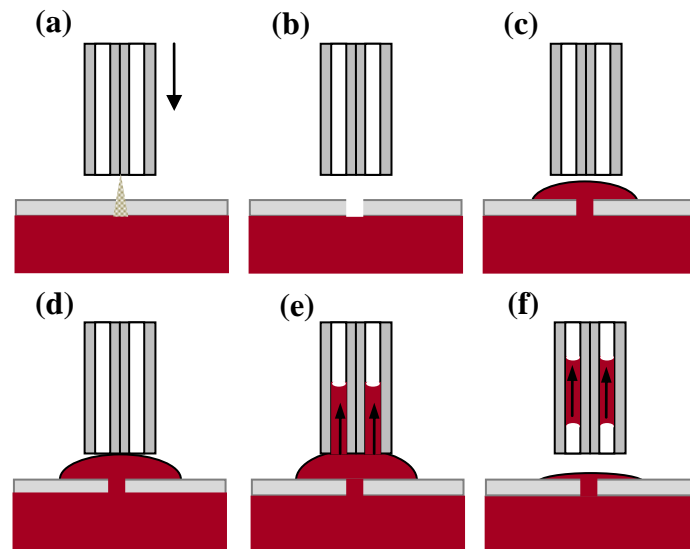


Fig. 3.7 Schematic illustration of both the ablation and the liquid collection process.

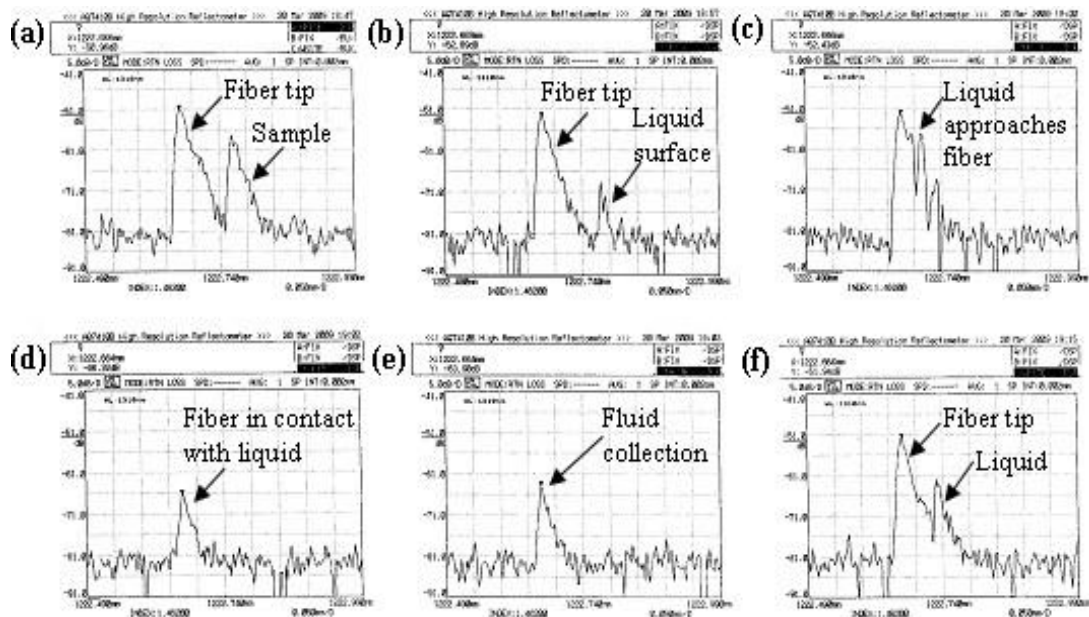


Fig. 3.8 The corresponding reflectometer traces of each step of the ablation and the liquid collection process shown in Fig. 3.7.

The fiber-tip was now brought towards the membrane of the liquid-filled cell and positioned $\sim 100 \mu\text{m}$ away from it, as seen in Fig. 3.7 (a) and with the corresponding reflectometer trace, as shown in Fig. 3.8 (a). Here, the ablation process is so rapid that it cannot be followed in real-time by the reflectometer, but, after ~ 1 second of ablation, the aluminum reflection decreased by more than 10 dB when an ablated hole had been created, as seen in Fig. 3.7 (b). The reflected signal from the liquid surface $\sim 120 \mu\text{m}$ away from the fiber-tip reflection is seen in Fig. 3.8 (b). Without changing the position of the fiber-tip the liquid goes through the ablated hole and forms a meniscus on the top of the membrane, as illustrated in Fig. 3.7 (c). The reflectometer trace of this situation is shown in Fig. 3.8 (c). When the liquid comes into contact with the fiber-tip, as shown in Fig. 3.7 (d), the signal amplitude decreases by ~ 13 dB, as seen in Fig. 3.8 (d) and (e), which also marks the beginning of the liquid collection, shown in Fig. 3.7 (e). When the fiber-liquid contact is broken, as illustrated in Fig. 3.7 (f), the fiber-tip reflected signal increases ~ 13 dB and the liquid surface reflection reappears, separated from the fiber-tip by $\sim 70 \mu\text{m}$, as seen in Fig. 3.8 (f). This completes the whole process for collecting the liquid sample.

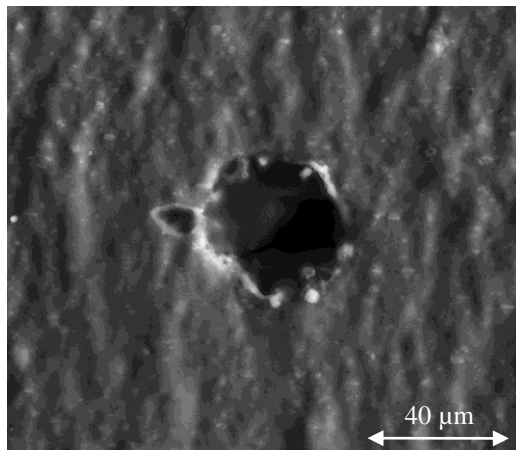


Fig. 3.9 SEM-image of the hole created in the aluminium platelet after being exposed to the laser irradiation.

Using a value for the fiber NA of 0.14 and a mode-field diameter of $8 \mu\text{m}$ at $1.06 \mu\text{m}$ wavelength, it is calculated (for a Gaussian approximation) that the beam diameter spreads to $27 \mu\text{m}$ on the aluminium target. However, the diameter of the circular hole created in the aluminum platelet is actually measured to be $\sim 40 \mu\text{m}$, implying that the size of the ablation area is approximately twice as wide as the size of the Gaussian spot, as seen in Fig. 3.9.

3.4 Discussion

Paper I describes how the three techniques discussed in this chapter have been combined in a successful way. However, there are some limitations to this method. The following problems should be addressed if this method is to be scaled-up for applications in life-sciences.

Low-coherence reflectometry is a good tool when the sample of study has good reflecting surfaces. If the sample of interest has surfaces with low reflectivity, then this method is not so appropriate for measuring distances.

Here, a naked fiber-tip was used as a probe. In reality, a naked fiber-tip is quite sensitive. It can easily break, get damaged, or be exposed to dirt and debris when being inserted in different environments. If the tip is too close to the material to be ablated, the tip can get dirty or even damaged by the material that is being removed during ablation. Hence, a non-flat fiber-tip will not only minimize the light delivery for ablation, but also minimize the light collection from the reflecting surfaces. The fiber-tip probe needs to be protected in some way and should possibly have a self-cleaning function in order to remove any dirt deposited on the fiber-tip surface.

A general problem, when dealing with fluidics in micrometer-sized holes and capillaries, is the potential for clogging of the holes. Here, in the present work, we have assumed that the liquid to be collected is clean and filtered. In reality, a real-world liquid can contain various particles that can clog up and even completely block the holes.

Chapter 4

Carbon-Coated Fiber for Fiber-Based Spectroscopy

Just because something doesn't do what you planned it to do doesn't mean it's useless.

- **Thomas A. Edison**

4.1 Motivation and Aim

It has been a common observation that laser excitation through a single-mode fiber for the collection of a low-intensity fluorescence signal could be affected by the background luminescence created by the primary-coating of the fiber and by the fiber itself [58-61]. This problem makes it difficult to measure low light-level signature, for example, from single-cells. The objective of this study is to reduce the luminescence from the polymer coating of a fiber using a special fiber with a nanometer-thick carbon layer on the cladding surface for applications in fiber-based spectroscopy. This is a detached field-of-study since these kinds of fibers are mainly used in harsh environments [23,24,7]. Because of the small cross-section of optical fibers, they can potentially be used as probes for Raman analysis and for single-cell spectroscopy.

Studies with multimode fibers show that luminescence increases with the fiber's numerical aperture (NA) [62] and the coating does not present a serious limitation. For small cores, on the other hand, the polymer coating is a source of noise and since it is necessary to increase the mechanical strength of the fiber, it is important to minimize the luminescence from the coating. The use of black epoxy resin adhesive and black teflon tubing on a section of an imaging fiber has also been reported to absorb the background radiation [63]. Work has also been done on reducing fiber background noise by choosing the glass type that gives minimal luminescence [61], using various types of optical interference filters to minimize the

fiber background [64,65] and by measuring the anti-Stokes Raman spectra at high-temperature, which eliminates fiber background mainly occurring in the Stokes Raman region [66].

The background luminescence significantly reduces the signal-to-noise ratio of a Raman-scattering measurement and, therefore, it can thwart the use of single-mode optical fibers for such measurements. The present study shows that, by coating the silica fiber with a thin layer of carbon, the background luminescence from the acrylate primary-coating is reduced, resulting in a 2-3 orders of magnitude improvement of the signal-to-noise (S/N) ratio. The S/N ratio is defined as the ratio between the mean value of the signal and the fluctuation (AC component) of the signal and the noise [67]. This sizable improvement in S/N will allow such fibers to be used as Raman probes for identifying various organic solvents.

4.2 Preliminary Studies

4.2.1 Experimental Setup

For the experiments performed in this work, a diode-pumped, solid-state laser (Cobolt Calypso 491) with an operating wavelength of 491 nm was used. The continuous-wave laser wavelength was generated by a sum-frequency mixing of 1064 nm and 914 nm radiation [68,69]. The laser light was reflected by a dichroic mirror and coupled into a ~ 2 m long optical test fiber using a 10x collimating lens. The test fiber output power was ~ 3 mW. The reflected luminescence in the fiber signal was transmitted by the dichroic mirror and passed a 7 mm thick yellow filter (OG515) to remove any reflected pump light. The beam was then focused by a 10x collimating lens into a 62.5 μm core multimode fiber and guided toward a 0.6 nm resolution cooled Ocean Optics spectrum analyzer (QE65000), with an operating range of 530-700 nm. The experimental setup is schematically illustrated in Fig. 4.1. The fiber in-coupling lens had a numerical aperture (NA) carefully chosen to maximize the coupling of the collimated laser light into the core of the test fiber. The lens then collimated the returning luminescence from the fiber core and not from the cladding. The remote tip of the test fiber was crushed to eliminate any reflections and it was seen that crushing the fiber tip repeatedly resulted in identical spectra.

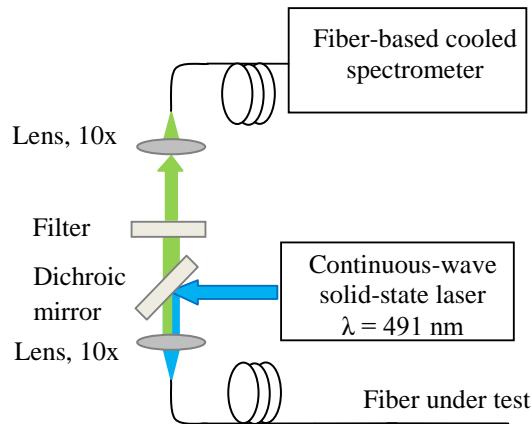


Fig. 4.1 Schematic illustration of the experimental setup for the fiber luminescence measurements.

For the experiments, four optical fibers were investigated: 1) A standard telecom germanium-doped-core fiber, 2) a similar germanium-doped-core fiber but with a carbon-coating, 3) a depressed-cladding pure-silica-core fiber, and finally 4) a depressed-cladding pure-silica-core fiber with a carbon-coating. All four fibers are single-mode at $1.5 \mu\text{m}$ wavelength but not at the pump laser wavelength (491 nm). The fibers have a numerical aperture (NA) in the range of 0.12-0.14. A more detailed description of the carbon-coated fibers is given in Section 2.1.2.

4.2.2 Fiber Coating Luminescence

A preliminary study was made on the luminescence from the primary-coating of the standard telecom germanium-doped-core fiber. This was done by illuminating the fiber that had a primary-coating from the side with a focused beam from the blue 491 nm laser. In this way, the luminescence from the coating can be measured without the unwanted contribution from the silica glass itself since the light is not propagating along the fiber. Fibers with an acrylate, a polyimide, and a low-index silicone-coating were illuminated from the side. The results of this luminescence study and the spectra of each polymer coating are shown in Fig. 4.2 (a) and (b). Since a majority of all the fibers, including the standard telecom fibers (STFs) have an acrylate primary-coating, the fibers chosen for this study were those with an acrylate coating. All four fiber types were illuminated from the side without the polymer coating in order to observe the amount of luminescence from the silica glass. The spectra of the naked fibers, shown in Fig. 4.2 (c), display a very flat and low-level background, illustrating that the silica fiber (with and without a carbon-coating) produces non-measurable luminescence.

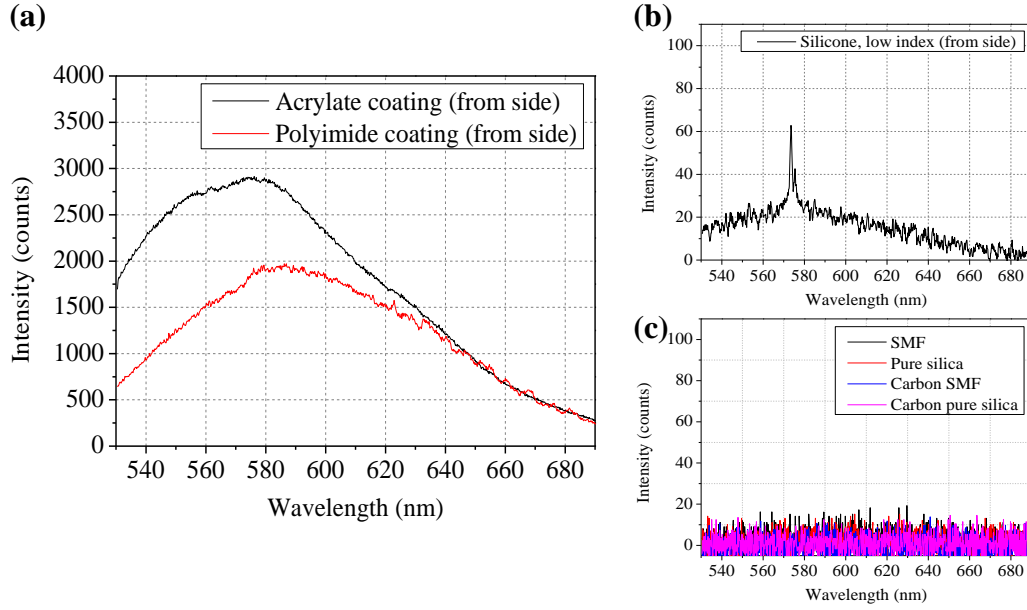


Fig. 4.2 Spectra of the polymer coating luminescence as measured from the side. (a) Acrylate- and polyimide-coated fibers, (b) low-index silicone-coated fiber and (c) various bare silica fibers.

4.2.3 Effect of the Carbon-Coating

Now, knowing the spectral shape from the acrylate primary-coating, the luminescence of the four fiber types were further studied with the laser light now focused into the core itself. The results are illustrated in Fig. 4.3. The spectra produced by the germanium-doped and the pure-silica fibers are dominated by the strong luminescence from the acrylate coating, as can be seen in Fig. 4.3 (a). Expanding the spectra and focusing on the carbon-coated fibers (with acrylate coating), a number of peaks are clearly seen, shown in Fig. 4.3 (b). In order to confirm that these luminescence peaks are from the glass itself, the primary-coating of the fibers were removed by immersing the fiber in hot sulfuric acid. Fig. 4.3 (c) shows the signals from the four naked fiber types; all of the signals are weak but of similar shape to the ones in the spectra, as seen in Fig. 4.3 (b). When comparing the black trace in Fig. 4.3 (a), where the light is propagating in the core, with that of the black trace in Fig. 4.2 (a), where an STF with acrylate coating is illuminated from the side, it can be seen that the signal intensity is ~ 4 times higher. Similarly, when comparing the traces of the naked fibers in Fig. 4.3 (c) with those in Fig. 4.2 (c), the signal intensity in Fig. 4.2 (c) is down into the noise level. Thus, the characteristic peaks of the silica fiber, as seen in Fig. 4.3 (c) cannot be distinguished.

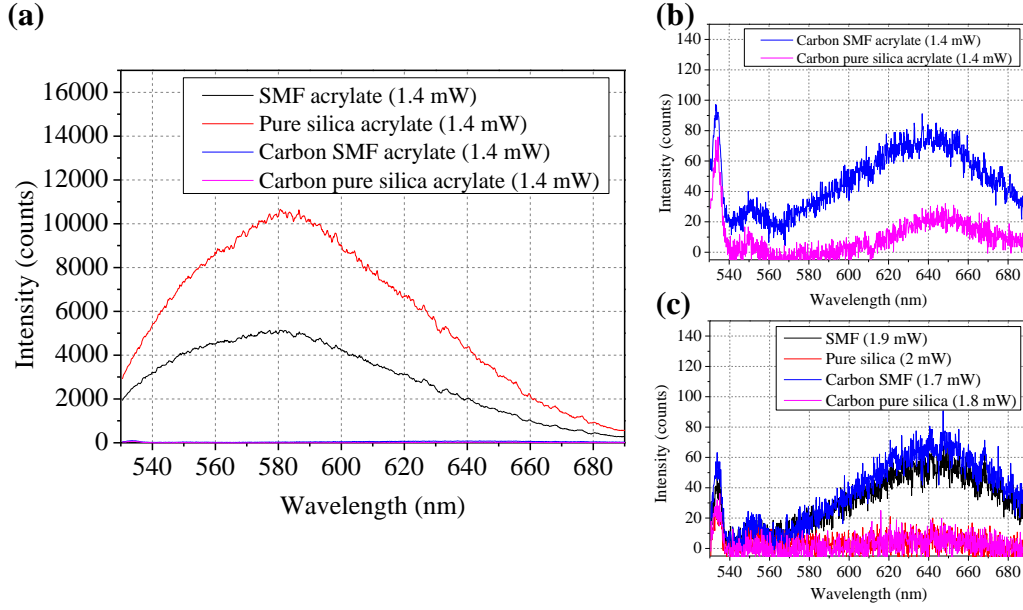


Fig. 4.3 Spectra of the fiber luminescence with (a) acrylate coating and (b) carbon-coated fiber with acrylate. (c) Measurements of the carbon-coated and non-carbon-coated fiber luminescence without the polymer coating.

In the absence of the polymer coating, the carbon-coated and the non-carbon-coated fibers show a luminescence signal quite similar to each other, indicating the presence of the same defect centers in the pure-silica fiber (100% silica core) and the germanium-doped fiber (97% silica core). The luminescence peaks seen in Fig. 4.3 are explained in Table 4.1. The wavenumbers corresponding to the wavelength shifts of the Raman peak are obtained using Eq. (4.1), where λ_{pump} is the pump wavelength and λ_{Raman} is the wavelength of the Raman peak:

$$Wavenumber [cm^{-1}] = \left(\frac{1}{\lambda_{pump}[cm]} - \frac{1}{\lambda_{Raman}[cm]} \right). \quad (4.1)$$

534 nm, 1640 cm^{-1}	Raman scattering in silica [70]
550 nm, 2184 cm^{-1}	Raman scattering in silica [70]
~ 580 nm	Acrylate
~ 650 nm	Non-bridging oxygen deficiency centers [71]

Table 4.1 Position and source of each luminescence peak as seen in the silica fibers.

It is also interesting to see how the luminescence is affected by the bending of the fibers into a loop of various radii, since in real-world applications sharp bends may be required. Of course, only fibers protected with a primary-coating can be bent sharply. Through sharp bending, more of the pump light in the cladding reaches the polymer coating, thus resulting in more and more coating luminescence [72]. The result of this study is described in detail in Paper II.

4.3 Experiments and Results

Being aware of the noise-reduction given by the carbon-coated fibers, the aim now was to use them as a Raman probe. The fiber tip was therefore cleaved and observed to be of good optical quality (and not crushed as in the previous experiments).

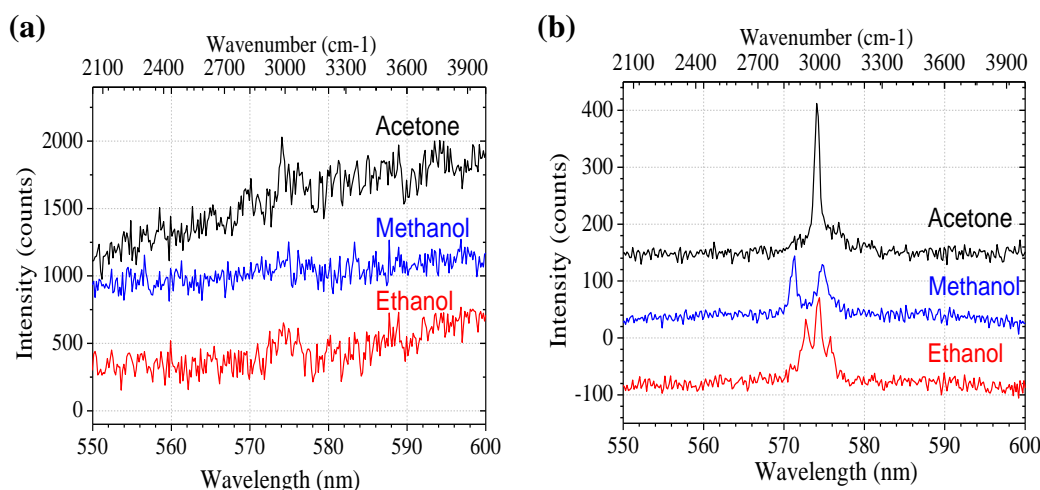


Fig. 4.4 Illustrations of (a) standard telecom fiber and (b) carbon-coated fiber used as a Raman probe.

Raman scattering spectra for acetone, methanol and ethanol were obtained by inserting a standard telecom fiber tip into these solvents. The expected Raman peaks between 570-580 nm, associated with a carbon-hydrogen vibrational mode, is barely distinguishable, as seen in Fig. 4.4 (a). The intensity recorded over the 10-second integration time in all measurements is large (above 50 000 counts). The noise here is proportional to the square root of the number of counts (~ 230), which is as expected [73]. The spectra obtained when the measurements are done with the carbon-coated fiber are shown in Fig. 4.4 (b) and the one, two and three spectral peaks, associated with acetone, methanol and ethanol, respectively, are clearly seen. Here, the noise level is ~ 10 times smaller than that of the signal, consistent with the square root relationship between the noise reduction and the number of counts (~ 15 counts). The acquisition time was 10 seconds in all of the experiments made. The 2-3 orders of magnitude improvement in signal-to-noise ratio is attributed to the elimination of the background luminescence caused by the acrylate coating.

4.4 Discussion

Much work has been done in developing fiber optical probes for Raman sensing within the life-science communities [74,75]. There are also many commercially available Raman probes in the market. These instruments typically exploit multimode fibers and employ multiple fibers for both the excitation and the collection of the Raman signal [76,77]. The method developed in this thesis project, where single-mode carbon-coated fibers have been exploited is not necessarily more advantageous than that based on probes employing multimode fibers, since a clear comparison between the two has not been made at this time. However, at single-cell levels, where the object under study is a few micrometers in dimensions, fibers with a small cross-section and a micrometer-size core will be preferable.

As can be seen in the present work, the background noise from the fiber itself (mainly from the silica fiber core) could not be reduced or entirely removed by the carbon-layer. In order to remove more of the background disturbance from the silica fiber, and to further increase the sensitivity (e.g., the S/N ratio), the background noise-level from the fiber core should be reduced with, for instance, a suitable filter. This is necessary for measuring at a single-cell level. However, background noise reduction of the silica fiber core was not explored in the present work

Chapter 5

Fiber-Based Optofluidic Components

Strength is the capacity to break a chocolate bar into four pieces with your bare hands, and then eat just one of the pieces.

- **Judith Viorst**

5.1 Motivation and Aim

The objective of the present work is to develop fiber-based components having in view their applications in the life-sciences. The fact that these components are hermitically sealed and have small cross-sections make them ideal for, e.g., minimally invasive diagnostics [7] or for sensing inside the body [5]. In principle, the optofluidic components described in the present work can be used with both liquids and gases, but the thesis work has mainly been involved in the handling of liquids. It was found that in order to exploit the microfluidic possibilities available in optical fibers with longitudinal holes, the liquid needs to be brought into the fiber without disturbing the light coupling or the light guidance, while at the same time light also needs to be coupled into the liquid without leakage, evaporation, or formation of bubbles and meniscus.

Several techniques have been reported for filling fluid into the holes of microstructured fibers. For instance, blocking cladding holes with a cured polymer [78], focused ion beam-milled microchannels on the side of the fiber [79], splicing with a lateral offset [80], using a micropipette [81], and C-shaped fiber for liquid delivery [82] are techniques that allowed for the interaction of a liquid-filled hollow core and light. However, the problem remains of how to collect or administer fluid in a controlled way without disturbing the optical path. In a research laboratory, it is possible to use non-ideal, bulky cells to couple light through lenses and pumps to fill the fiber with the liquid. However, for future clinical use, a more user-friendly

arrangement is required. Having all-fiber components fully-spliced would thus be an advantage, in the sense that light would be coupled in and out through conventional fibers, the liquids would correspondingly be handled by conventional capillaries and the light/liquid interaction is made to take place in a very small-volume protected environment.

5.2 Various Fiber Arrangements

The fiber arrangements described in this chapter exploit silica fiber capillaries and microstructured fibers as was described in Section 2.1.1. These fiber arrangements will deliver light with low-loss and can either be used for the collection or for the delivery of the fluid through the longitudinal side-holes of the fiber.

5.2.1 Microstructured Fiber with Etched Telecom Fiber

A microstructured fiber, for instance, a 4-hole fiber, was spliced to a standard telecom fiber (STF) with similar core-size but with a smaller external diameter ($\sim 50 \mu\text{m}$), obtained by etching a short section of the fiber. The remaining fiber length was kept at the standard $125 \mu\text{m}$ diameter. The etched section was then cleaved and spliced to the 4-hole fiber with $< 0.1 \text{ dB}$ optical loss. It is, of course, possible to use a $50 \mu\text{m}$ outer-diameter telecom fiber in order to avoid etching altogether, but it was preferred to use $125 \mu\text{m}$ fibers for the optical coupling. Also, by etching many fibers at once the effort needed per component were reduced.

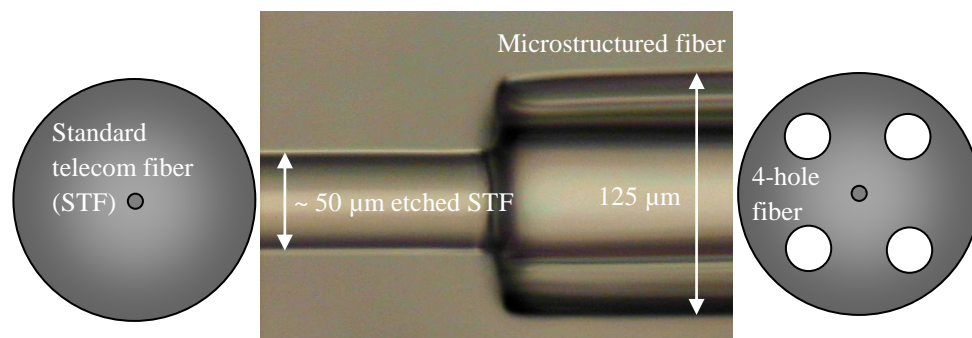


Fig. 5.1 Microscope image of the fiber arrangement, where the microstructured fiber was spliced to a short piece of etched standard telecom fiber.

This fiber arrangement, illustrated in Fig. 5.1 and, being the setup used in the experiments described in Section 3.3, it allows for light delivery with minimal optical loss. It is also a convenient way to allow for the liquid collection, e.g., by the capillary forces in the side-holes of the fiber without having to access the holes from the side. However, this arrangement does not permit each fiber side-hole to be accessed individually.

5.2.2 “Billys”

In the arrangement described here as “Billys”, schematically illustrated below in Fig. 5.2, the liquid delivery to the microstructured fiber is performed in an especially attached capillary, which has an inner-diameter of $127\ \mu\text{m}$ and an outer-diameter of $250\ \mu\text{m}$. A single hole of length $\sim 1\ \text{mm}$ is opened in the capillary by side-polishing. An etched piece of STF is inserted through this hole longitudinally into the capillary. This makes it possible to bring in the light from the side of the arrangement after the splicing to, in this case, a 4-hole fiber. The etched section of the telecom fiber is slightly bent inside the $250\ \mu\text{m}$ capillary. The small bend, however, is largely determined by the length of the side-hole opened in the capillary. Experimentally, the measured loss induced by this bend is $< 0.1\ \text{dB}$.

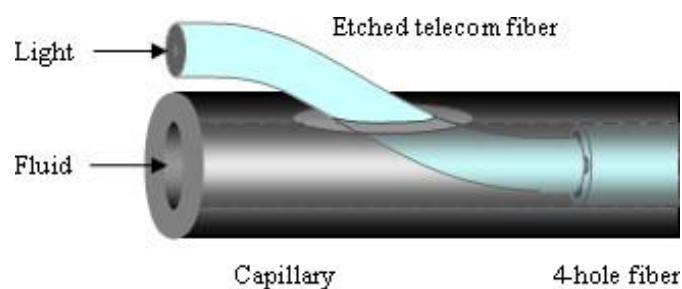


Fig. 5.2 Schematic illustration of the “Billys” fiber arrangement.

To prevent any fluid leakage from the polished opening of the capillary, a suitable adhesive (e.g., UV curing glue Vitralit 2009 F) was used to seal the opening entirely after the insertion. The liquid is delivered from the capillary into the non-blocked area of the fiber side-holes. The existing $\sim 2\ \mu\text{m}$ gap, between the microstructured fiber surface and the inner wall of the capillary, needs to be closed to prevent liquid leakage. This can be done by using a suitable adhesive or by collapsing the capillaries slightly.

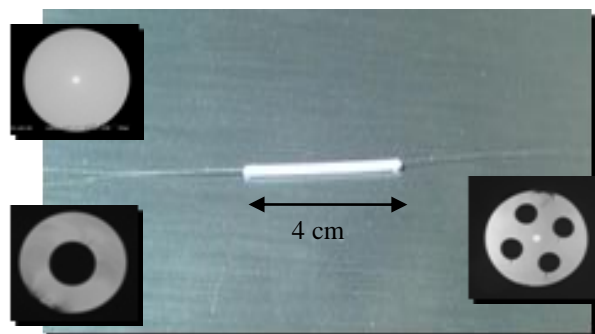


Fig. 5.3 Image of the “Billys” fiber arrangement accommodated inside a splice protector. On the left side, of the “Billys”, it has a standard telecom fiber for light in-coupling and a capillary for fluid delivery, and on the right side there is a microstructured 4-hole fiber, where the light and fluid is combined in the fiber.

In cases where smaller sample volumes are required, it is possible to reduce the capillary hole-size by, for instance, inserting a 125 μm outer-diameter capillary with a $\sim 50 \mu\text{m}$ hole into the 250 μm capillary. The encompassing capillary can, in this case, be made short ($\sim 3 \text{ cm}$). This arrangement, illustrated in Fig. 5.3, is accommodated inside a conventional splice protector, which has on one side a 4-hole fiber for light and fluid delivery and, on the other side, an STF and a capillary fiber.

5.2.3 Individual Access of Fiber Side-Holes

An advantage of using microstructured fiber with several side-holes, e.g., a 2-hole fiber or a 4-hole fiber, is the possibility of using each side-hole for the collection and/or the delivery of different kinds of fluids. It can be assumed that the microstructured fiber is used for the light coupling as well as for the fluid handling and would, therefore, be spliced to a non-etched STF. The splice covering the entire end area of the microstructured fiber would, of course, prevent fluid flow in the side-holes. Accessing each side-hole is then accomplished by polishing the microstructured fiber from the side at various positions of the fiber, as illustrated in Fig. 5.4 (a).

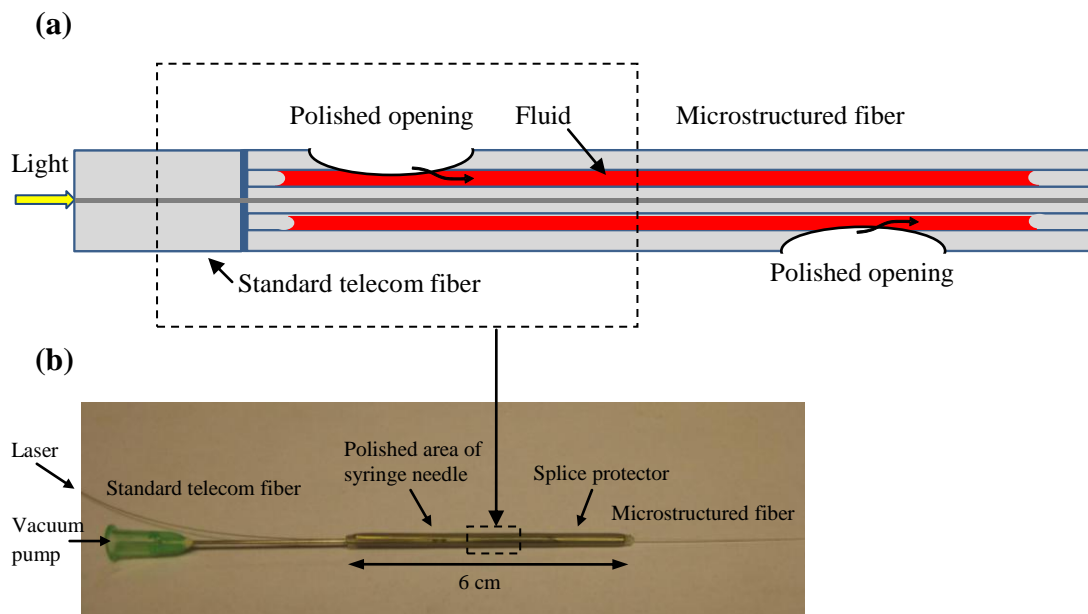


Fig. 5.4 Schematic illustration of accessing individual fiber side-holes (a) by polishing the fiber from the side. The fluid here is illustrated in red. (b) The fiber arrangement is inserted into a syringe needle to allow for controlled fluid handling.

Here, the fluid is illustrated in red. The spliced STF with the polished microstructured fiber is inserted from the side into a syringe needle with a polished side-opening. The fiber section with the splice and the polished opening is positioned inside the needle. The section of the needle with the polished opening is accommodated inside a splice protector, as illustrated in Fig. 5.4 (b). Each polished

fiber side-hole can be protected in this way, hence, allowing for individual fluid handling (using an applied pressure difference). The fiber arrangement described in Section 5.2.1 can be inserted into a syringe needle in the same way, which would allow the fiber arrangement to be used with controlled fluid handling.

5.2.4 Principle of “2-1-2”

When feeding a liquid into a capillary, problems such as meniscus formation, dripping and/or evaporation can occur. Coupling light into a liquid-filled capillary where there already is a meniscus present would lead the in-coupled light to refract. Since such an effect is unwanted, there is a need of liquid handling in a controlled way and for a structure that would eliminate the issues described above. By employing a fiber arrangement, such as that illustrated in Fig. 5.5, the problems with meniscus formation, evaporation and dripping would entirely be eliminated. Here, in this design, a microstructured fiber is spliced to a capillary or a hollow-core fiber with a relatively large central hole. After splicing, this hole collects the fluid from the microstructured fiber, and becomes a liquid-core in which the light will propagate. This liquid-collecting capillary could, in turn, be spliced to an even narrower hollow-core capillary or a photonic crystal fiber (PCF) resulting in a narrow liquid-core fiber, where light can propagate in the fluid. The length of the intermediate liquid-collecting capillary should be kept as short as possible ($< 50 \mu\text{m}$) to keep the optical losses small (discussed more in detail in Section 5.3). The length of the liquid-core section can range from as short as $\sim 20 \mu\text{m}$ to up to meters-long. Here, if a meniscus is formed it would be in the microstructured fiber side-holes and not in the liquid core section of the arrangement, as can be seen in Fig. 5.5.

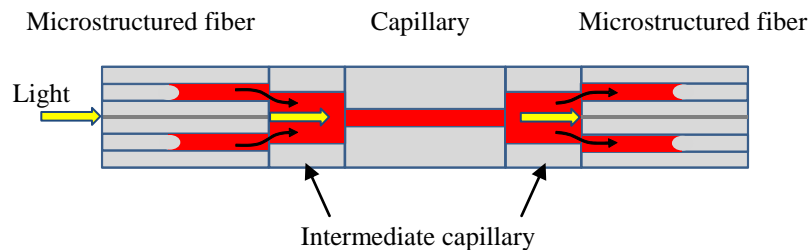


Fig. 5.5: Schematic illustration of a “2-1-2” fiber arrangement, which allows light to be coupled into a fluid-core without bubbles or meniscus formation. The intermediate capillary sections should be kept short $< 50 \mu\text{m}$ to minimize the optical loss.

5.3 Fully-Spliced All-Fiber Component

Fig. 5.6 illustrates a complete optofluidic component designed to combine light and fluid in an integrated form. The component can be liquid-filled (without bubbles or meniscus formation) or be used with a continuous fluid flow without disturbing the optical coupling. Evanescent field interaction between the light and the fluid can take place if the fiber side-holes are sufficiently close to the core. However, the interaction becomes much more efficient by allowing the light to propagate longitudinally in the fluid. Here, the “Billys” arrangement is combined with the “2-1-2” fiber arrangement.

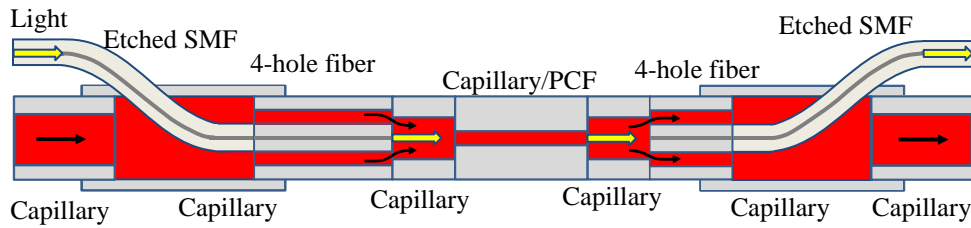


Fig. 5.6 Schematic illustration of a fiber-based optofluidic component.

The optical losses of this combined liquid-core section depend very strongly on the refractive indices involved, the scattering and the absorption of the fluid used. The optical loss in the intermediate capillary in air is measured by increasing the separation between the two solid-core fibers (carbon-coated fibers, CCF), as seen in Fig. 5.7. By keeping the length of the intermediate capillary short, e.g., 20 μm , the measured loss was $6 \pm 3\%$ and, for the 50 μm case, the loss was $18 \pm 3\%$. These values show relatively good agreement with those estimated from a Gaussian beam approximation [83], which works well for a standard fiber core [84].

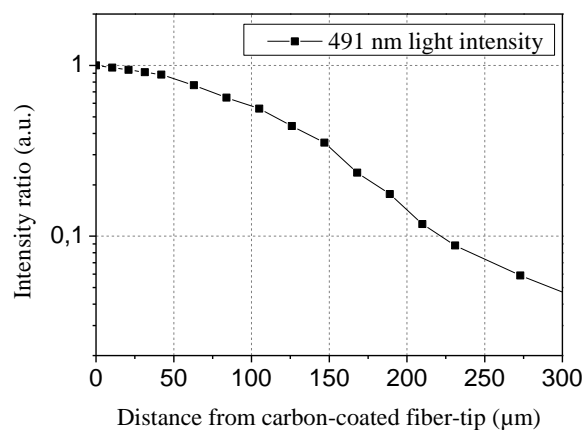


Fig. 5.7 Optical loss in air due to the distance between two solid-core fibers; here two carbon-coated fibers (CCFs) are used.

5.4 Discussion

In the present work, the benefits of dealing with micrometer dimensions for the handling of small sample-volumes have been discussed. However, when down-scaling in size, parameters such as flow speed is greatly reduced since the flow is mainly laminar in microdevices. In this sense, it would not be possible to compete with standard flow cytometries, for instance, where the detection speed is 1000 particles per second. Also, since the inside of the fiber arrangements cannot easily be processed, it becomes difficult to introduce a smooth interface between a fiber spliced to a capillary. This affects the fluid flow behavior in the sense that stagnant zones might appear. In the present work, a deeper investigation has not been made regarding stagnant zones. But, in order to exploit these fiber arrangements to the fullest extent for analysis of biological species, the fibers need to be tailored for this specific purpose. Clogging of the holes because of clustered particles, for instance, could be a potential problem. Also, if the liquid sample has air bubbles and is introduced into the fiber arrangement, this will disturb the fluid flow in a negative way. However, these practical issues are quite typical for microdevices in general but should, nevertheless, be addressed if the fiber arrangements are to be applied in the life-sciences.

Chapter 6

Detection and Isolation of Micrometer-size Particles in a Fiber

*No one who achieves success does so without acknowledging the help of others.
The wise and confident acknowledges this help with gratitude.*

- *Alfred North Whitehead*

6.1 Motivation and Aim

Exploiting some of the results described earlier in the thesis, the objective of the work in the present chapter is to develop a method for the detection and the collection of micrometer-size particles into a hollow optical fiber. Here, a microstructured optical fiber with longitudinal side-holes is exploited for the excitation, identification, and the collection of particles and species considered of interest. The excitation light comes through the fiber from a blue laser source (491 nm). The identification is performed by choosing the particles that luminesce at the appropriate wavelength. When a particle of interest is sufficiently near the fiber-tip, a suction system is activated for the collection of the particle into the fiber side-hole.

This technique finds applications in the selection of rare particles in fluids and for *in-vivo* collection of cells. The backwards guidance of the optical signal allows for real-time continuous study of the environment through, for instance, Raman scattering or fluorescence excitation. The longitudinal holes that are introduced in the cladding of the microstructured fiber multiply the degrees of freedom available. They can be exploited for the collection and retrieval of different species of interest for further analysis. They can also be used *in-vivo* for the delivery of, for instance, medicine to a specific region in the human body.

6.2 Preliminary Studies

6.2.1 Experimental Fibers

Microstructured fibers with either one or two side-holes were used in the experiments for the present work. Microstructured fibers are described in more detail in Section 2.1.1. The 1-hole fiber, as seen in Fig. 6.1 (a) below, has a 32 μm diameter side-hole and the core-to-hole center distance, D_1 , is also 32 μm . The 2-hole fiber, seen in Fig. 6.1 (b), has two symmetrically located 25 μm diameter side-holes. Here, the core-to-hole center distance, D_2 , is 29 μm .

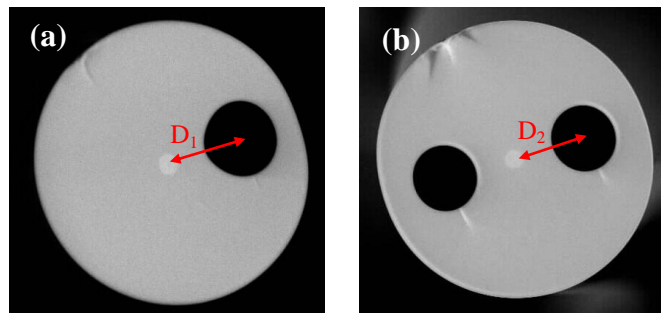


Fig. 6.1 SEM-images of the 125- μm diameter microstructured fibers used in this work. Illustrations of (a) the 1-hole fiber with a 32 μm diameter side-hole and (b) the 2-hole fiber with 25 μm diameter side-holes.

In most of the experiments, the 2-hole fiber was preferred, as it was easier to obtain low-loss splices with this fiber. The splice-loss between a standard telecom fiber (STF) and a 2-hole fiber is typically ~ 0.1 dB, while between a 1-hole fiber and an STF, the loss is ~ 1 dB. This is because of, when splicing a 1-hole fiber to, for instance, a standard single-mode fiber (SMF28), the single fiber hole of the 1-hole fiber slightly collapses, which results in a displacement of the 1-hole fiber core and a mismatch to the SMF28 core.

Results from the measurements that were performed in Paper II have shown that for fluorescence studies, a carbon-coated fiber was preferred, since it greatly reduced the background luminescence from the polymer-coating of the fiber. Here, a microstructured fiber with a carbon-layer on the cladding would have been preferable. But, since such a fiber was not available, the carbon-coated fiber was spliced to a piece of 2-hole fiber. The fiber arrangement used for the experiments was prepared as described in Section 5.2.3 above.

Fig. 6.2 below illustrates two alternative methods for controlling the fluid in the fiber using an applied pressure difference. First, an STF spliced to a 2-hole fiber with a polished side-opening and positioned on a glass slide is described. Another piece of glass that was used as a lid was placed above the fiber with some silicone glue in between, which created a hermetic enclosure of the fluid. Two syringe needles were then placed between the glass slides for inlet and outlet of the fluid, as seen in

Fig. 6.2 (a). The arrangement was convenient in that it allowed for easy visual inspection, but the preparation time was quite long since the curing time of the silicon glue was ~ 1 day. The arrangement, which is described in more detail in Section 5.2.3, and seen in Fig. 6.2 (b), had a much shorter preparation time and was, therefore, more preferable.

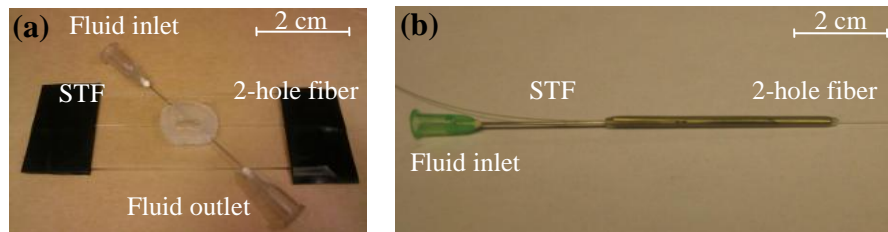


Fig. 6.2 (a) and (b) are images of the two methods for controlling the fluid inside a microstructured fiber as described in the text.

6.2.2 Detection of fluorescence

The setup for fluorescence detection is shown in Fig. 6.3 (a)¹ below. A compact, low noise, sum-frequency mixed, diode-pumped solid-state laser emitting at 491 nm was used for the excitation [68,69]. The light was coupled to a piece of carbon-coated fiber (CCF), which was used to deliver the excitation light and guide the collected fluorescent signal from the particle sample. The excitation beam was launched into the fiber core through a dichroic beam splitter and a 10x focusing lens, and propagated through the fiber. The output power at the fiber-tip was ~ 3 mW.

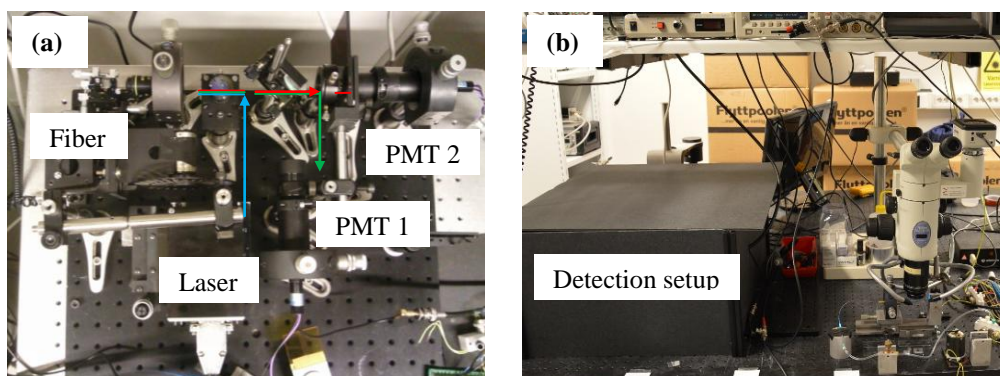


Fig. 6.3 (a) Photo of the detection setup and (b) the “black box” containing the sensitive parts of the system. In this way, background noise from the surrounding environment was reduced.

¹ In Fig. 6.3 (a), two photomultiplier tubes can be seen, which means that the setup can in principle be used for the detection of multiple fluorescence wavelengths when excited with the same pump laser. However, in the present work only one detector was used.

The fluorescence emission from the excited particles was guided backwards through the fiber, transmitted through the beam-splitter, and finally detected by a photomultiplier tube (PMT). The backward-scattered laser radiation and the stray light were filtered out using an interference filter and a color filter, placed before the PMT, to ensure that only the fluorescence from the particles was detected. The fluorescence signal was displayed using a regular oscilloscope. To reduce the background noise from the surrounding laboratory environment, the experimental setup was placed inside a “black box”, as seen in Fig. 6.3 (b).

When a fluorescent particle was in front of the fiber-tip, two effects occurred simultaneously. First, the pump laser intensity decayed with distance because the pump beam spread out spatially. The second effect was that the luminescence from the particle that was collected by the core also depended strongly on the separation between the particle and the fiber-tip. In Fig. 6.4, a schematic illustration of the situation of the pump laser light from the fiber including the various variables for determining the fluorescence detection and collection, is shown.

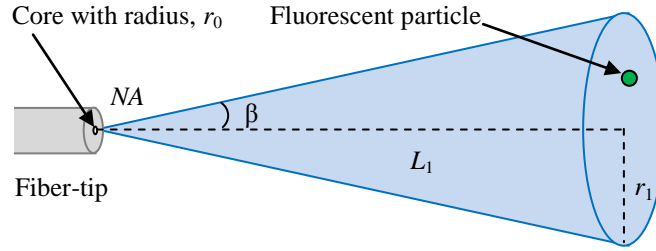


Fig. 6.4 Schematic illustration of the beam spread and the illuminated light area from a standard telecom fiber.

Here, r_0 is the fiber core radius and the illuminated radius, r_1 , is defined as $r_1 = r_0 + L_1 \tan(\beta)$. The angle, β , is defined as one half of the light-acceptance-angle, determined by the numerical aperture (NA) of the fiber. The intensity is expressed as $I = P/A_1$, where A_1 is the area and P is the total output power from the fiber. The intensity at the fiber-tip, I_0 , is then expressed as $I_0 = P/r_0^2$ and the intensity at a distance L_1 from the fiber-tip, I_1 , is written as $I_1 = P/r_1^2$. The intensity ratio can then be described as $I_1/I_0 = r_0^2/r_1^2$, and I_1 can, therefore, be rewritten in the following way:

$$I_1 = I_0 \left[\frac{r_0}{r_0 + L_1 \tan(\beta)} \right]^2. \quad (6.1)$$

For an SMF28, r_0 is 4 μm and $\tan(\beta)$ is 0.13 and 0.1 when the surrounding medium is either air and water, respectively. The angle β is, thus, 7.35° and 5.52° in air and in water, respectively. If, for instance, the NA is zero, meaning that the beam is non-diverging, then $I_1 = I_0$ for any length L_1 . And, on the other hand, if L_1 is very large compared with the fiber radius the intensity falls with the square of the distance, as can be seen in Fig. 6.5 below:

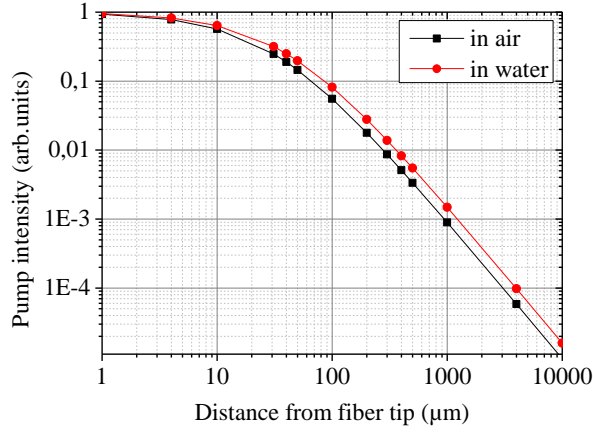


Fig. 6.5 The pump laser intensity falls off with distance from the fiber-tip. The black and red trace represents the situation when the surrounding medium of the fiber is air and water, respectively.

We now assume that the fluorescence is homogeneous, isotropically radiating in all directions, and that the particle is a point source. The illuminated spherical area is described as $4\pi r_{part}^2$, shown in Fig. 6.6 below, where r_{part} is the radius of the sphere and can be expressed as $r_{part} = (r_0^2 + l^2)^{1/2}$. Here, l is the distance between the particle and the center of the fiber-tip surface. We now calculate the power incident on a cap which comprises the fiber core of radius, r_0 , as seen in Fig. 6.6. The spherical area of the cap, A_{cap} , is defined as $A_{cap} \cong \pi(r_0^2 + h_c^2)$, where the height, h_c , is defined as $h_c = r_{part} - l$. The area of the cap may be further expressed as $A_{cap} \cong \pi r_0^2 + \pi((r_0^2 + l^2)^{1/2} - l)^2$.

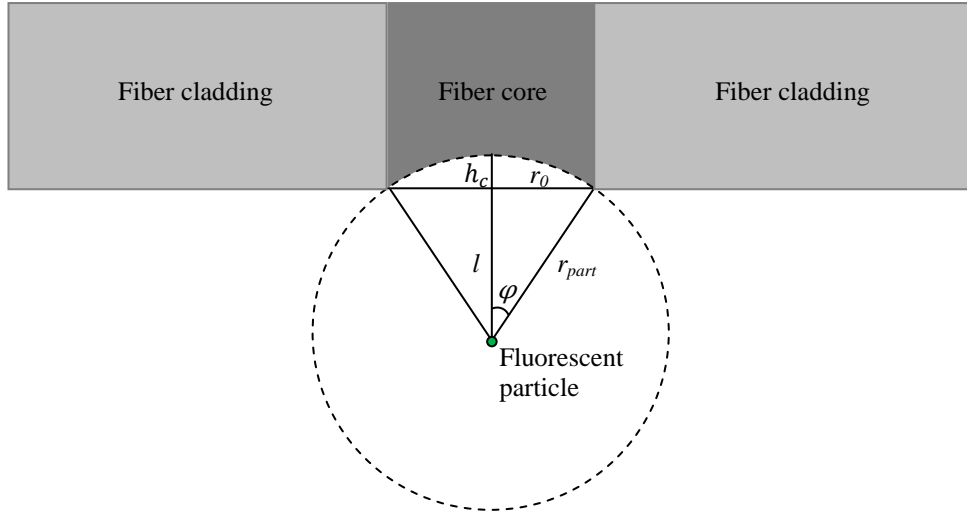


Fig. 6.6 Schematic illustration of the emitted fluorescence from a particle situated in front of the fiber-tip.

Assume first that the particle is far from the fiber-tip surface ($l \sim r_{part}$), and the illuminating angle φ is very small, much smaller than the acceptance angle of the

fiber given by the NA . In this case, all rays reaching the core surface πr_0^2 are collected and guided back by the fiber to the detector. The fraction of the power reaching the core, may then be expressed as the ratio between the small area of the cap and the spherically illuminated area from the particle, and can be written in the following way:

$$\frac{I_1}{I_0} = \frac{r_0^2 + ((r_0^2 + l^2)^{1/2} - l)^2}{4(l^2 + r_0^2)}. \quad (6.2)$$

If one assumes that the distance l is very large compared with the core radius ($l \gg R_0$), one can neglect the difference between l and r_{part} ($l \sim r_{part}$), and, that consequently $h_c = 0$. In this case, the fraction of the collected intensity reduces to $r_0^2/4l^2$. This goes with the inverse of the square of the distance between the particle and the fiber. However, when this distance is comparable with the core radius ($l \sim r_0$), the angle comprised by the cap may exceed the numerical aperture of the fiber. Then, it is necessary to consider that the signal collection is saturated at a maximum angle given by the NA of the fiber, even if the particle is very close to the fiber core. The illumination angle, φ , is given by $\varphi = \tan^{-1}(r_0/l)$, which gives that as long as $\tan^{-1}(r_0/l_{air}) \leq 7.35^\circ$ in air and $\tan^{-1}(r_0/l_{water}) \leq 5.52^\circ$ in water, all of the light impinging on the fiber core will be guided to the detector. If $\tan^{-1}(r_0/l_{air}) > 7.35^\circ$ in air and $\tan^{-1}(r_0/l_{water}) > 5.52^\circ$ in water, then some light will be lost. Thus, the collection efficiency saturates at the value of $r_0/l_{air} = 0.13$ in air and $r_0/l_{water} = 0.1$ in water, respectively. For an SMF28 with a core radius of $4 \mu\text{m}$, the largest distance for maximum collection is $31 \mu\text{m}$ in air and $40 \mu\text{m}$ in water. If the particle is closer to the fiber-tip than $31 \mu\text{m}$ in air or $40 \mu\text{m}$ in water, the signal collected and guided to the photodetector does not increase above that for $31 \mu\text{m}$ in air or $40 \mu\text{m}$ in water, respectively, as can be seen in Fig. 6.7 below.

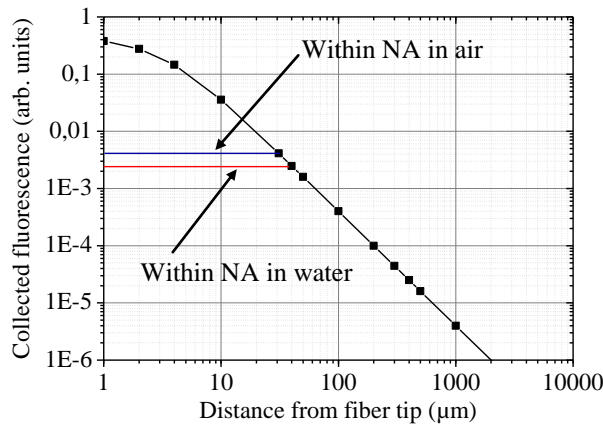


Fig. 6.7 The graph shows the amount of fluorescence emitted from a particle with various distances between the fiber-tip and the particle at maximum fluorescence collected into the fiber in air (blue line) and in water (red line).

Finally, if one combines the efficiency of the excitation with that of the collection, both of which fall off rapidly with the distance, the total efficiency can be

calculated, as shown below in Fig. 6.8 (a) for air and (b) for water, respectively. For large values of l , the efficiency decreases with the fourth power of the distance ($\propto 1/l^4$). One conclusion from this estimate is that the total collection efficiency goes down relatively slowly up to about 31 μm in air and around 40 μm in water, respectively but then, between 31 μm and 100 μm (in air) and between 40 μm and 100 μm (in water), the fluorescence efficiency reduces about 50 times. This means that the trigger level should be set so that only the particles within the nearest 30 μm (in air) or 40 μm (in water) can trigger the system. Another conclusion is that the signal detected from particles about 1 mm away from the fiber is approximately 10^4 times weaker than that of particles 100 μm from the fiber-tip. Even in the absence of scattering and absorption, the luminescence from distant particles can, therefore, be neglected.

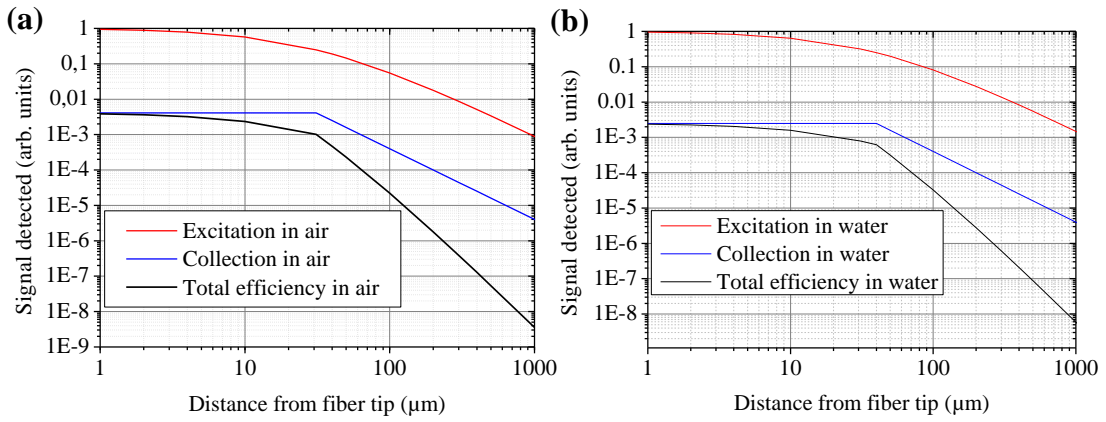


Fig. 6.8 The excitation, the collection and the total efficiency of the signal from a fluorescent particle in (a) air and (b) water, respectively.

6.2.3 Collection of the liquid in the fiber

In order to guarantee adequate particle collection, a minimum volume of liquid needs to be retrieved through the longitudinal fiber hole. A particle facing the core at a distance, L_{coll} , or less, produces a fluorescence signal capable of triggering the sample collection. In order to guarantee the retrieval of this particle, a liquid volume confined in a sphere of radius, R_{coll} , should be collected into the capillary, where approximately half of this volume is occupied by the fiber. In this approximation, the estimated volume is given by Eq. (6.3) below. The collection radius, r_{coll} , can be determined from the expression $r_{coll}^2 = L_{coll}^2 + D^2$.

$$V = \left(\frac{2\pi}{3}\right) (L_{coll}^2 + D^2)^{3/2}. \quad (6.3)$$

To minimize the collected volume, and hence increase the concentration of the collected target particles, it is important to design the geometry of the hole and the core so that they are as near to each other as possible. For the fiber geometry used, the

retrieved volume depends strongly on the distance D between the side-hole and the core, as seen in Fig. 6.9.

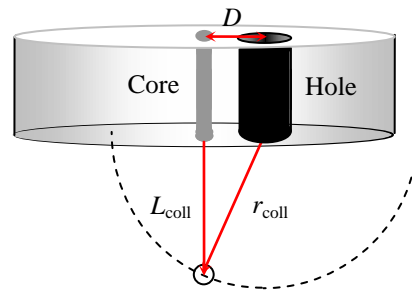


Fig. 6.9 Illustration of the variables required for determining the minimum collection volume.

A preliminary study to calibrate the suction of liquid as a function of pump-opening time was made using the liquid collection into a capillary alone (without the detection part). The liquid collected in this measurement was filtered distilled water. The collection was carried out using a 39 cm long capillary with 25 μm inner-diameter placed inside a syringe needle, which in turn was connected to a solenoid valve. The valve was connected to a vacuum pump and a computer controlling the opening/closing of the valve. The valve was pre-set to mechanically open/close for various times, up to 800 milliseconds. The shortest time for the valve to open/close was 40 milliseconds. The pump employed, could be set to different under-pressure values. Here, an applied pressure difference of 0.1, 0.15, 0.2, and 0.25 bar were tested. The results of the liquid collection into the capillary with various pressures are illustrated in Fig. 6.10 below. The collection volume (based on the collected liquid length in the capillary) can be determined by the expression, $V_{fiber} = d_{coll}\pi r_{cap}^2$, where r_{cap} is the capillary hole radius and d_{coll} is the collected liquid length in the capillary.

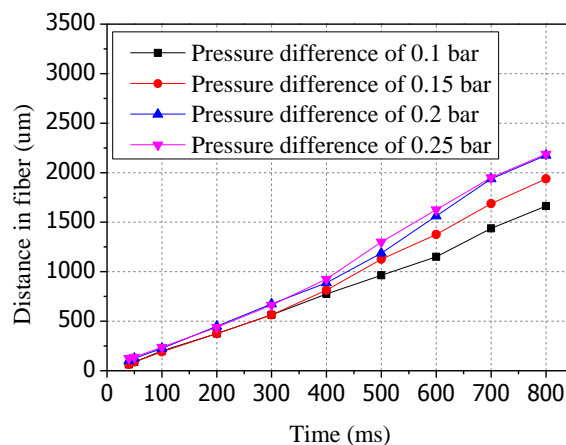


Fig. 6.10 Results showing the liquid collection into a 25 μm inner-diameter capillary, with various valve open/close times for calibration purpose.

Next, a measurement was performed exploiting a microstructured fiber with a polished 25 μm side-hole in a fiber arrangement such as was described in Section

5.2.3. The experiment was performed under similar conditions as the previous collection experiment above. However, the applied pressure difference used here was set to only 0.25 bar. In Fig. 6.11 below, the red trace shows the measurements exploiting a 39-cm long microstructured fiber and the blue one with a 24 cm long piece of fiber, respectively. It can be seen, for instance, that when the length was reduced by 1.63 times, (e.g., 39/24), the flow reduced 1.55 times (e.g., 2300/1480) at the time of 500 milliseconds. It is also seen that the red and the blue lines do not pass through the origo without “adding” an unexpected bend for the shortest opening times. This collection behavior is most likely caused by the fiber arrangement itself. Here, a fiber was inserted from the side in a syringe needle (as described in Section 5.2.3), hence, disturbing a part of the flow reaching the fiber side-hole.

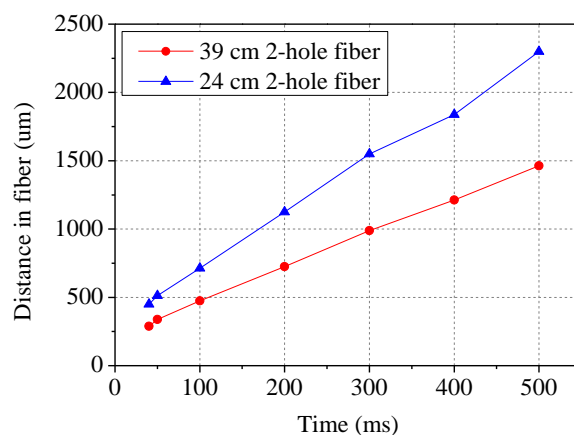


Fig. 6.11 Liquid collection measurements using the fiber arrangement described in Section 5.2.3.

6.3 Experiments and Results

In this section, a demonstrated proof-of-principle method to detect and collect micrometer-size fluorescent beads using a fiber-optic probe and laser-induced fluorescence (LIF) will be described. The fiber-based detection system not only allowed for continuous *detection*, but also for the *collection* of the detected beads. The light was launched down through the fiber into the sample volume with the excited particles supposedly located in the proximity of the fiber-tip. The fluorescence returned through the fiber to the detector triggered a small pump, which sucked the beads into the side-hole of the fiber. The LIF detection method used here could potentially be exchanged or combined with Raman or other scattering detection methods.

The experimental setup, as shown in Fig. 6.12 (a) below, was similar to the one discussed in Section 6.2.2. However, the electrical signal from the photomultiplier tube (PMT) was now digitized in a 12 bit A/D converter and sent to the computer for trigger-decision instead of being displayed on an oscilloscope. A

solenoid valve was connected to the vacuum pump employed with the fiber arrangement, as shown in Fig. 6.12 (b). The valve was controlled with the help of a LABVIEW program to automatically open/close when the fluorescence signal exceeded a trigger level, i.e., indicating a particle to be collected close to the fiber hole. The syringe needle (containing the fiber arrangement) was easily connected to a vacuum pump to allow for the sample collection in the fiber using the applied pressure difference. In this way, the liquid flow was allowed in the 24-cm long microstructured fiber without disturbing the guidance of the optical light and without having any risks of leakage or for contamination. The fiber arrangement employed can in principle be re-used if it is cleaned/washed properly and if it is not damaged.

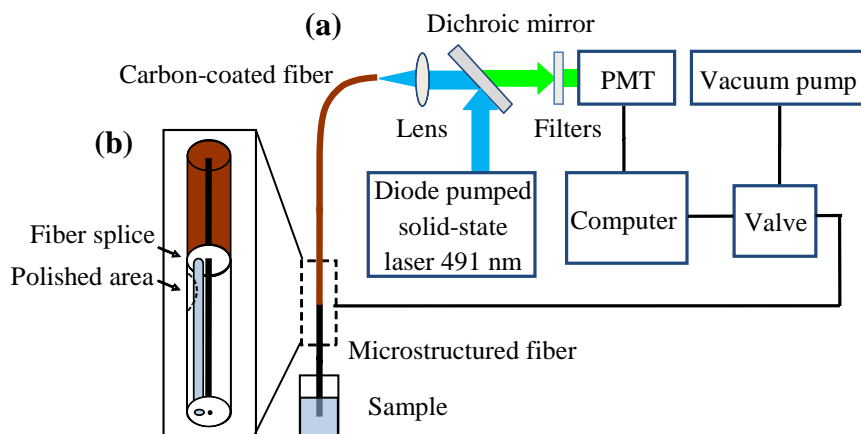


Fig. 6.12 Schematic illustration of the experimental setup for the detection and the collection of the micrometer-size particles. (a) The general block diagram of the setup and (b) the detailed view of the carbon-coated fiber spliced to the polished 1-hole fiber.

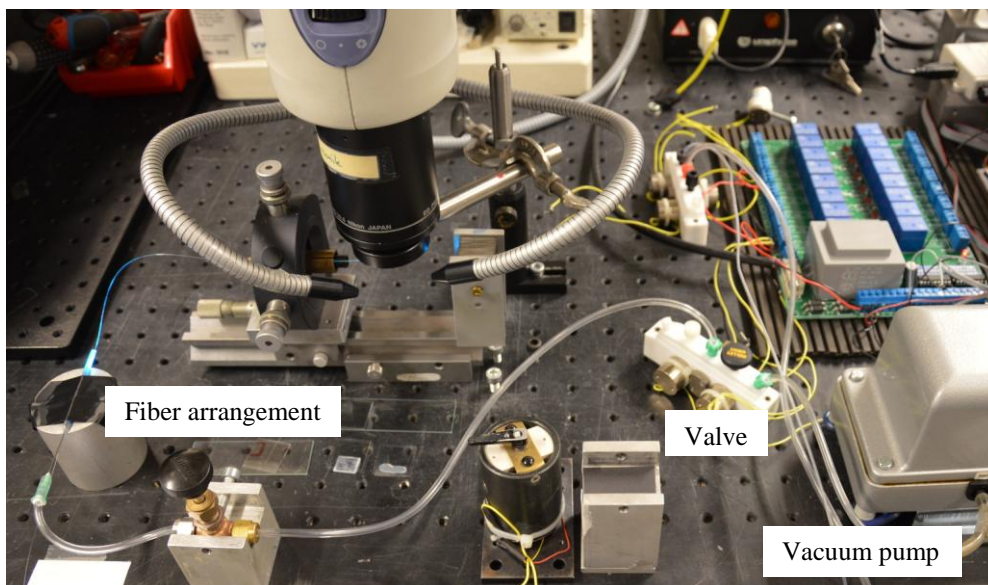


Fig. 6.13 Photographic image of the fiber arrangement, which is connected to a solenoid valve, which, in turn, is connected to the vacuum pump. A computer controlled the open/close periods of the valve.

Fig. 6.13 illustrates the particle collection part of the experiment. Since this part was not sensitive to background light, it was not necessary to confine it in the “black box”, seen in Fig. 6.3 (b), which contained the sensitive part of the experimental setup. The fiber from the detection unit was taken out from the “black box” and was positioned in a container with a sample solution. A microscope was used for the visualization of the collection process.

In the following experiment, the detection and the collection of the 5 μm diameter polystyrene beads (Firefli™ Fluorescent Green, with a maximum excitation wavelength of 468 nm and an emission at 508 nm) were made from a small-volume liquid solution in a container. The amplitude of the signal varied with the distance of the fiber core to the beads. In order to keep the specificity high, only signal peaks with intensity value > 5 (a.u.) were considered of interest, which then became the trigger-level. The bead, was here $\sim 40 \mu\text{m}$ away from the fiber-tip, which was considered the maximum distance between the fiber-tip and the particles that still would give a maximum fluorescence collection (as discussed in Section 6.2.2); this distance corresponded to a collection radius of $\sim 50 \mu\text{m}$. This is estimated to be equal to an average collection volume of around 0.3 nanoliter. According to the liquid collection measurements, for a 24-cm long microstructured fiber, as was shown in Fig. 6.11 above, this collection volume was equal to a liquid collected distance of $\sim 0.5 \text{ mm}$ in the fiber side-hole, which again corresponded to an open/close valve time of 40 milliseconds.

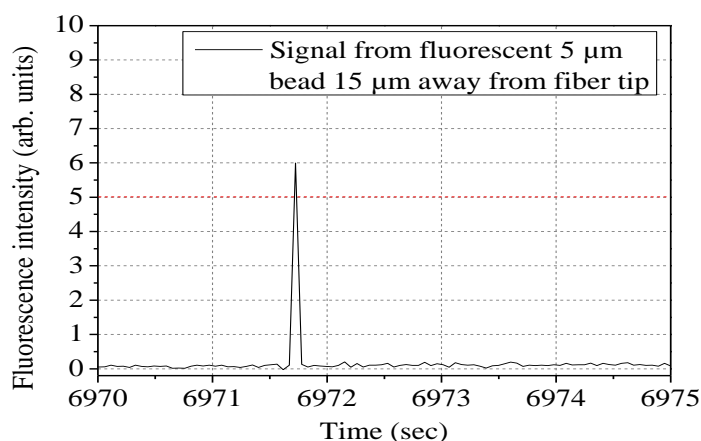


Fig. 6.14 The fluorescence signal of a detected bead $\sim 15 \mu\text{m}$ away from the microstructured fiber-tip. The trigger-level (marked in red) was pre-set to a fluorescence intensity value of 5 (a.u.).

It was observed that the beads could be isolated without other beads being collected, assuming that the beads were equally distributed in the sample. However, the concentration of the bead sample should be lower than $3 \cdot 10^6$ beads per milliliter, which means that there should not be more than about 1 bead within the 0.3 nanoliter collection volume. Whenever the fluorescence signal was above the pre-set signal threshold, the LABVIEW program automatically opened the valve connected to the

vacuum pump for 40 milliseconds. Fig. 6.14 illustrates a typical signal from a bead that was located $\sim 15 \mu\text{m}$ away from the fiber-tip and yielded a signal magnitude of > 5 (a.u.) on the preset scale, thus triggering the suction system. The collected beads inside the fiber-hole can barely be seen in Fig. 6.15 below.

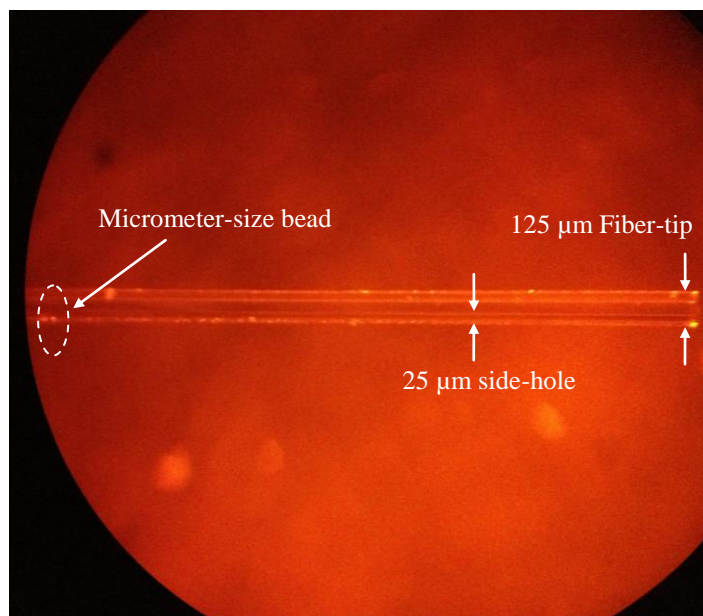


Fig. 6.15 Microscope image of a collected $5 \mu\text{m}$ diameter bead inside the fiber-hole.

6.4 Discussion

The fiber-based LIF system introduces the possibility to detect single, micrometer-size, fluorescent samples in a liquid medium and isolate the single samples from the homogeneous sample solutions. In the case where a dilution of the sample is allowed, one can aim at an increase of the sample concentration in the fiber, as the trigger level can be set for only collecting particles that are within the collection radius, r_{coll} (introduced in Section 6.2.3).

The use of a single fiber for illumination and collection as exploited in this work, where, for instance, the core-to-hole center distance of $D = 29 \mu\text{m}$, can be compared with the case when the illuminating fiber is placed in the close neighbourhood of a capillary with an outer diameter of $125 \mu\text{m}$. Increasing D to a distance of $125 \mu\text{m}$ would mean ~ 15 times increase of the minimum collection volume. In other words, in order to guarantee the retrieval of the wanted species when a standard $125 \mu\text{m}$ fiber is used for illumination and detection, and an independent $125 \mu\text{m}$ capillary is used for the fluid collection, one needs to collect a volume ~ 15 times larger, according to Eq. (6.3), than if the hole-to-core distance is $29 \mu\text{m}$. The use of microstructured fibers is thus highly advantageous.

Chapter 7

Conclusions

*Everyone is a genius at least once a year.
The real geniuses simply have their bright ideas closer together.*
- **Georg C. Lichtenberg**

7.1 Summary

Optical fibers can transmit signals bi-directionally, nominally without cross-talk. In the thesis, this ability has been exploited for sensing purposes. An excitation signal has been sent into a fiber, and the collected reflected light has been used for monitoring the environment in front of the fiber core. It has been shown that the reflected signal from an optical fiber can be monitored in real-time, for instance, for measuring the distances to scattering objects and for continuous detection of low-level Raman signals (in Paper II) and fluorescence excitation (in Paper IV) from the surrounding environment.

It has been shown, in Paper I, that optical fibers, in spite of their micrometer-size core, can be exploited for the delivery of high-power laser light for ablation of specific materials. The small size of an optical fiber is very advantageous when the power needed to be delivered, at hard-to-reach places and with a minimum disturbance of the surrounding environment. Also, the positioning of the fiber in the ablation process can be performed using the fiber in the monitoring system.

The longitudinal holes introduced into the microstructured fiber are (in Paper IV), used both for the collection and the retrieval of laser-induced fluorescence, detecting single micrometer-size particles that are considered being of interest. It has also been shown, in Paper III, that microstructured fibers and capillaries can be exploited in various all-fiber arrangements for combining light and fluids. This

increases the functionality of optical fibers substantially. These all-spliced fiber-based components are not only promising for life-science applications, but can also be applied in other fields where there exist a need to combine light and fluid(s) in a controlled way.

Finally, by introducing a nanometer thick layer of carbon on the cladding surface of a single-mode fiber, we have shown (in Paper II) that the background luminescence due to the polymer coating of the fiber is reduced by 2-3 orders of magnitude. This results in an increased sensitivity for fiber-based spectroscopy, which is beneficial for measuring low-level signals. In principle, this technique can be combined with microstructured fibers to optimize their performance.

7.2 Outlook

Several improvements can be made in all of the experimental setups described in this thesis. While in this report the aim was to make proof-of-principle demonstrations, the various techniques and setups can be further tailored and optimized for more specific life-science applications. For example, in the present work not much time was spent on the fluid delivery process through the side-holes of the microstructured fiber. This can be further exploited in future life-science applications. For instance, one might find it important to deliver a specific medicine to various non-accessible locations in the body or for the injection of (minute amounts of) chemical or biological substances *in-vivo* on demand. Thereby, one is able to induce chemical and/or biological reactions and one can also combine them with local photochemistry. This kind of fiber functionality should be further explored, as well as trying to use each of the side-holes in, for instance, a 4-hole fiber individually, for collection of different types of particles and bionic samples.

The all-spliced fiber arrangements should, if possible, be more tailored for the collection/delivery of biological species. This means that the processing of the fibers and the capillaries should be improved, for example, by making smoother transitions between their inner-walls to avoid fluidic hindrances such as stagnant zones.

This work, finally, has exploited some of the degrees of freedom that optical fibers exhibit, such as longitudinal holes in the cladding for the fluidics, light absorbing coatings, and for the optical delivery to and from the samples for demonstrating new practical functionalities in optical fibers for life-science applications

References

- [1] S. E. Miller and A. G. Chynoweth, "Optical fiber telecommunications," Academic Press Inc., London (1979).
- [2] S. A. Boppart, T. F. Deutsch, and D. W. Rattner, "Optical imaging technology in minimally invasive surgery," *Surgical endoscopy*, **13**, 718–722 (1999).
- [3] B. Lau, R. A. McLaughlin, A. Curatolo, R. W. Kirk, D. K. Gerstmann, and D. D. Sampson, "Imaging true 3D endoscopic anatomy by incorporating magnetic tracking with optical coherence tomography: proof-of-principle for airways," *Optics Express*, **18**, 27173-27180 (2010).
- [4] S. A. Boppart, B. E. Bouma, C. Pitris, G. J. Tearney, J. G. Fujimoto, and M. E. Brezinski, "Forward-imaging instruments for optical coherence tomography," *Optics Letters*, **22**, 1618-1620 (1997).
- [5] S. Rehman and Å. Claesson, "Specialty optical fibers make surgery less invasive," *BioPhotonics*, October (2011).
- [6] G. B. Hocker, "Fiber-optic sensing of pressure and temperature," *Applied Optics*, **18**, 1445-1448 (1979).
- [7] A. Mendez and T. F. Morse, *Specialty Optical Fibers Handbook*, Academic Press (2006).
- [8] A. Katzer, "Lasers and optical fibers in medicine," Academic Press Inc., San Diego (1993).
- [9] J. Hecht, "City of light – the story of fiber optics," Oxford University Press, New York (2004).
- [10] C. Kao and G. A. Hockham, "Dielectric-fibre surface waveguides for optical frequencies," *IEE Proceedings*, **133**, 191-198 (1986).
- [11] F. A. Jenkins and H. E. White, "Fundamentals of optics," McGraw-Hill Kogakusha Ltd., Tokyo (1965).
- [12] Corning SMF28 Optical Fiber, Product information on Corning website: <http://www.corning.com/WorkArea/showcontent.aspx?id=57655>
- [13] J. Stone, "Optical Transmission Loss in Liquid-Core Hollow Fibers," *IEEE Journal of Quantum Electronics*, March, 386-388 (1972).
- [14] A. G. Ewing, R. A. Wallingford, and T. M. Olefirowicz, "Capillary electrophoresis," *Analytical Chemistry*, **61**, 292-303 (1989).
- [15] C. Monat, P. Domachuk, and B. J. Eggleton, "Integrated optofluidics: A new river of light," *Nature Photonics*, **1**, 106-114 (2007).
- [16] P. Domachuk and B. J. Eggleton, "Fiber-based optofluidics," *Proceedings of SPIE*, **6588**, 65880C1-65880C12 (2007).

- [17] P. Mach, M. Dolinski, K. W. Baldwin, J. A. Rogers, C. Kerbage, R. S. Windeler, and B. J. Eggleton, "Tunable microfluidic optical fiber," *Applied Physics Letters*, **80**, 4294-4296 (2002).
- [18] P. Domachuk, H. C. Nguyen, and B. J. Eggleton, "Transverse probed microfluidic switchable photonic crystal fiber devices," *IEEE Photonics Technology Letters*, **16**, 1900-1902, (2004).
- [19] K. Kieu, L. Schneebeli, R. A. Norwood, and N. Peyghambarian, "Integrated liquid-core optical fibers for ultra-efficient nonlinear liquid photonics," *Optics Express*, **20**, 8148-8154 (2012).
- [20] D. Lopez, O. Tarasenko, and W. Margulis, "All-fiber Kerr cell," *Optics Letters*, **37**, 3288-3290 (2012).
- [21] P. Russell "Photonic crystal fibers," *Science*, **299**, 358-362 (2003).
- [22] J. C. Knight, "Photonic crystal fibres," *Nature*, **424**, 847-851 (2003).
- [23] E. A. Lindholm, J. Li, A. S. Hokansson, and J. Abramczyk, "Low speed carbon deposition process for hermetic optical fibers," in *Proceedings of International Wire and Cable Symposium (IWCS)*, 1999.
- [24] J. Li, E. A. Lindholm, J. Horska, and J. Abramczyk, "Advances in design and development of optical fibers for harsh environments" (Specialty Photonics, 1999).
http://specialtyphotonics.com/about/white_papers/Harsh%20Environs.pdf
- [25] A. Tomita and P. J. Lemaire, "Hydrogen-induced loss increases in germanium-doped single-mode fibers," *Electronics Letters*, **20**, 512-514 (1985).
- [26] D. A. Pinnow, G. D. Robertson, Jr., and J. A. Wysocki, "Reduction in static fatigue of silica fibers by hermetic jacketing," *Applied Physics Letters*, **34**, 17-19 (1979).
- [27] G. M. Whitesides, "The origins and the future of microfluidics," *Nature*, **442**, 368-373 (2006).
- [28] S. Nagrath, L. V. Sequist, S. Maheswaran, D. W. Bell, D. Irimia, L. Ulkus, M. R. Smith, E. L. Kwak, S. Digumarthy, A. Muzikansky, P. Ryan, U. J. Balis, R. G. Tompkins, D. A. Haber, and M. Toner, "Isolation of rare circulating tumour cells in cancer patients by microchip technology," *Nature*, **450**, 1235-1239 (2007).
- [29] G. Falkovich, "Fluid mechanics," Cambridge University Press, New York, (2011).
- [30] T. M. Squires and S. R. Quake, "Microfluidics: Fluid physics at the nanoliter scale," *Reviews of Modern Physics*, **77**, 977-1026 (2005).

- [31] D. J. Biebe, G. A. Mensing, and G. M. Walker, "Physics and applications of microfluidics in biology," *Annual Review of Biomedical Engineering*, **4**, 261-286 (2002).
- [32] B. J. Kirby, "Micro- and nanoscale fluid mechanics," Cambridge University Press, New York (2010).
- [33] H. A. Stone and S. Kim, "Microfluidics: Basic issues, applications and challenges," *AIChE Journal*, **47**, 1250-1254 (2001).
- [34] Y. Fainman, L. P. Lee, D. Psaltis, and C. Yang, "Optofluidics: Fundamentals, devices and applications," McGraw-Hill Companies Ltd., U.S.A. (2010).
- [35] D. Psaltis, S. R. Quake, and C. Yang, "Developing optofluidic technology through the fusion of microfluidics and optics," *Nature*, **442**, 381-386 (2006).
- [36] M. J. Gordon, X. Huang, S. L. Pentoney, Jr., and R. N. Zare, "Capillary electrophoresis," *Science*, **242**, 224-228 (1988).
- [37] H. H. Gilgen, R. P. Novák, R. P. Salathé, W. Hodel, and P. Beaud, "Submillimeter optical reflectometry," *Journal of Lightwave Technology*, **7**, 1225-1233 (1989).
- [38] G. Chartier, "Introduction to optics," Springer Science, U.S.A. (2005).
- [39] A. Vogel and V. Venugopalan, "Mechanisms of pulsed laser ablation of biological tissues," *Chemical Reviews*, **103**, 577-644 (2003).
- [40] M. N. R. Ashfold, F. Claeysens, G. M. Fuge, and S. J. Henley, "Pulsed laser ablation and deposition of thin films," *Chemical Society Reviews*, **33**, 23-31 (2004).
- [41] G. L. LeCarpentier, M. Motamedi, L. P. McMath, S. Rastegar, and A. J. Welch, "Continuous wave laser ablation of tissue: Analysis of thermal and mechanical events," *IEEE Transactions on Biomedical Engineering*, **40**, 188-200 (1993).
- [42] K-H. Leitz, B. Redlingshöfer, Y. Reg, A. Otto, and M. Schmidt, "Metal ablation with short and ultrashort laser pulses," *Physics Procedia*, **12**, 230-238 (2011).
- [43] H. J. Schwarz and H. Hora, "Laser interaction and related plasma phenomena," Plenum Press, New York (1974).
- [44] M. Forrer, M. Frenz, V. Romano, H. J. Altermatt, H. P. Weber, A. Silenok, M. Istomyn, and V. I. Konov, "Bone-ablation mechanism using CO₂ lasers of different pulse duration and wavelength," *Applied Physics*, **56**, 104-112 (1993).
- [45] A. Charlton, M. R. Dickinson, T. A. King, and A. J. Freemont, "Erbium-YAG and Holmium-YAG laser ablation of bone," *Lasers in Medical Science*, **5**, 365-373 (1990).

- [46] Z. Z. Li, J. E. Code, and W. P. Van De Werme, "Er:YAG laser ablation of enamel and dentin of human teeth: Determination of ablation rates of various fluences and repetition rates," *Lasers in Surgery and Medicine*, **12**, 625-630 (1992).
- [47] A. Oraevsky, R. Esenaliev, S. Jacques, and F. Tittel, "Mechanism of precise tissue ablation with minimal side-effect," *Proceeding of SPIE*, **2323**, 250-261 (1995).
- [48] M. Cristofanilli, D. F. Hayes, G. T. Budd, M. J. Ellis, A. Stopeck, J. M. Reuben, G. V. Doyle, J. Matera, W. J. Allard, M. C. Miller, H. A. Fritsche, G. N. Hortobagyi, and L. W. M. M. Terstappen, "Circulating tumor cells: A novel prognostic factor for newly diagnosed metastatic breast cancer," *Journal of Clinical Oncology*, **23**, 1420-1430 (2005).
- [49] J. A. Flint, Y. T. Van Duynhoven, F. J. Angulo, S. M. DeLong, P. Braun, M. Kirk, E. Scallan, M. Fitzgerald, G. K. Adak, P. Sockett, A. Ellis, G. Hall, N. Gargouri, H. Walke, and P. Braam, "Estimating the burden of acute gastroenteritis, foodborne disease, and pathogens commonly transmitted by food: An international review," *Clinical Infectious Diseases*, **41**, 698-704 (2005).
- [50] M. A. Schwarz and P. C. Hauser, "Recent developments in detection methods for microfabricated analytical devices," *Lab on a Chip*, **1**, 1-6 (2006).
- [51] R. L. McCreery, "Raman spectroscopy for chemical analysis," John Wiley & Sons, U.S.A. (2005).
- [52] A. Y. Fu, C. Spence, A. Scherer, F. H. Arnold, and S. R. Quake, "A microfabricated fluorescence-activated cell sorter," *Nature Biotechnology*, **17**, 1109-1111 (1999).
- [53] M. Sauer, J. Hofkens, and J. Enderlein, "Handbook of fluorescence spectroscopy and imaging," WILEY-VCH Verlag GmbH & CO, Weinheim (2011).
- [54] C. V. Raman and K. S. Krishnan, "A new type of secondary radiation," *Nature*, **121**, 501-502 (1928).
- [55] Ando Electric Co., Ltd., Japan, AQ 7410B High-resolution reflectometer, Product information:
<http://support.us.yokogawa.com/downloads/TMI/COMM/AQ7410/aq7410be.pdf>
- [56] S. M. Klimentov, S. V. Garnov, T. V. Kononenko, V. I. Konov, P. A. Pivovarov, and F. Dausinger, "High rate deep channel ablative formation by picosecond-nanosecond combined laser pulses," *Applied Physics A.*, **69** [Suppl.], S633-S636 (1999).

- [57] S. Zoppel, R. Merz, J. Zehetner, and G. A. Reider, "Enhancement of laser ablation yield by two color excitation", *Applied Physics A.*, **81**, 847–850 (2005).
- [58] M. Gallagher and U. Österberg, "Spectroscopy of defects in germanium-doped silica glass," *Journal Applied Physics*, **74**, 2771-2778 (1993).
- [59] S. Kannan, M. E. Fineman, and G. H. Sigel, Jr., "Defect-related luminescent patterns in bulk silica and optical fibers stimulated by sub-band gap (248 nm) excimer laser radiation," *Journal of Luminescence*, **60**, 433-436 (1994).
- [60] T. F. Cooney, H. T. Skinner, and S. M. Angel, "Comparative study of some fiber-optic remote Raman probe designs. Part II: tests of single-fiber, lensed, and flat- and bevel-tip multi-fiber probes," *Applied Spectroscopy*, **50**, 849-860 (1996).
- [61] E. Schartner, H. Ebendorff-Heidepriem, and T. Monro, "Sensitive fluorescence detection with microstructured optical fibers," *Proceedings of SPIE*, **8028** (2011).
- [62] J. Ma and Y. S. Li, "Fiber Raman background study and its application in setting up optical fiber Raman probes," *Applied Optics*, **35**, 2527-2533 (1996).
- [63] C. J. de Lima, S. Sathaiyah, L. Silveira, Jr., R. A. Zângaro, and M. T. T. Pacheco, "Development of catheters with low fiber background signals for Raman spectroscopic diagnosis applications," *Artificial Organs*, **24**, 231-234 (2000).
- [64] M. L. Myrick and S. M. Angel, "Elimination of background in fiber-optic Raman measurements," *Applied Spectroscopy*, **44**, 565-570 (1990).
- [65] R. B. Thompson, M. Levine, and L. Kondracki, "Component selection for fiber-optic fluorometry," *Applied Spectroscopy*, **44**, 117-122 (1990).
- [66] S. Dai, J. E. Coeffield, G. Mamantov, and J. P. Young, "Reduction of fused-silica-fiber Raman backgrounds in high-temperature fiber-optic Raman spectroscopy via the measurement of anti-Stokes Raman spectra," *Applied Spectroscopy*, **48**, 766-768 (1994).
- [67] www.hamamatsu.com, "PHOTOMULTIPLIER TUBES, basics and applications," Hamamatsu Photonics (2007).
http://www.hamamatsu.com/resources/pdf/etd/PMT_handbook_v3aE-Chapter4.pdf
- [68] M. Stjernström, F. Laurell, and H. Brismar, "Diode-pumped solid state laser light sources for confocal laser scanning fluorescence microscopy," *Journal of Laser Applications*, **20**, 160 (2008).

- [69] J. Nordborg and H. Karlsson, "Multiline DPSS lasers – a true Ar-ion alternative," (EuroPhotonics, June/July, 2004).
http://www.cobolt.se/Filer/dokument/europhotonics_dual-calypto_july04_cobolt.pdf
- [70] R. H. Stolen, C. Lee, and R. K. Jain, "Development of the stimulated Raman spectrum in single-mode silica fibers," *Journal of Optical Society of America B*, **1**, 652-657 (1984).
- [71] G. H. Sigel, Jr., and M. J. Marrone, "Photoluminescence in as-drawn and irradiated silica optical fibers: an assessment of the role of non-bridging oxygen defect centers," *Journal of Non-Crystalline Solids*, **45**, 235-247 (1981).
- [72] M. L. Myrick, S. M. Angel, and R. Desiderio, "Comparison of some fiber optic configurations for measurement of luminescence and Raman scattering," *Applied Optics*, **29**, 1333-1344 (1990).
- [73] www.photometrics.com, "Keep the noise down! Low noise: An integral part of high-performance CCD (HCCD) camera systems," Technical note (2010).
<http://www.photometrics.com/resources/technotes/pdfs/snr.pdf>
- [74] A. Wax, M. G. Giacomelli, T. E. Matthews, M. T. Rinehart, F. E. Robles, and Y. Zhu, "Optical spectroscopy of biological cells," *Advances in Optics and Photonics*, **4**, 322–378 (2012).
- [75] P. Matousek and M. D. Morris, "Emerging Raman applications and techniques in biomedical and pharmaceutical fields," Springer, Berlin Heidelberg (2010).
- [76] U. Utzinger and R. R. Richards-Kortum, "Fiber optic probes for biomedical optical spectroscopy," *Journal of Biomedical Optics*, **8**, 121-147 (2003).
- [77] T. F. Cooney, H. T. Skinner, and S. M. Angel, "Comparative study of some fiber-optic remote Raman probe designs. Part I: model for liquids and transparent solids," *Applied Spectroscopy*, **50**, 836-848 (1996).
- [78] Y. Huang, Y. Xu, and A. Yariv, "Fabrication of functional microstructured optical fibers through selective-filling technique," *Applied Physics Letters*, **85**, 5182-5184 (2004).
- [79] C. M. B. Cordeiro, C. J. S. de Matos, E. M. dos Santos, A. Bozolan, J. S. K. Ong, T. Facincani, G. Chesini, A. R. Vaz, and C. H. Brito Cruz, "Towards practical liquid and gas sensing with photonic crystal fibres: side access to the fibre microstructure and single-mode liquid-core fiber," *Measurement Science Technology*, **18**, 3075-3081, (2007).
- [80] W. Qian, C. Zhao, Y. Wang, C. C. Chan, S. Liu, and W. Jin, "Partially liquid-filled hollow-core photonic crystal fiber polarizer," *Optics Letters*, **36**, 3296-3298 (2011).

- [81] R. M. Gerosa, D. H. Spadoti, C. J. S. de Matos, L. de S. Menezes, and M. A. R. Franco, "Efficient and short-range light coupling to index-matched liquid-filled hole in a solid-core photonic crystal fiber," *Optics Express*, **19**, 24687-24698 (2011).
- [82] S. Hosseinzadeh Kassani, J. Park, M. Park, and K. Oh, "Sensitivity enhancement of in-line chemical sensing device with C-type fiber and photonic crystal fiber," *Proceedings of SPIE*, **8237**, 82371Z (2012).
- [83] CVI Melles Griot, "Gaussian beam propagation," *CVI Melles Griot Technical Guide*, Vol. 2, Issue 2, 2-5 (2009).
- [84] A. M. Kowalevich, Jr., and F. Bucholtz, "Beam divergence from an SMF-28 optical fiber," Naval Research Laboratory report NRL/MR/5650--06-8996 (2006).